ACS Sustainable Chemistry & Engineering

pubs.acs.org/journal/ascecg

Perspective

# Electrospun Lignin-Derived Carbon Micro- and Nanofibers: A Review on Precursors, Properties, and Applications

Efstratios Svinterikos, Ioannis Zuburtikudis,* and Mohamed Al-Marzouqi

Cite This: *ACS Sustainable Chem. Eng.* 2020, 8, 13868–13893

Read Online

ACCESS | Metrics & More | Article Recommendations

**ABSTRACT:** The development of advanced engineering materials from low-cost renewable or waste resources is a key aspect of sustainability. Carbon nanofibers (CNFs) are a one-dimensional form of carbon with diameters in the submicron- and in the nanometer range with wide applicability in energy storage, catalysis, and adsorption. Lignin has recently emerged as a low-cost, biorenewable precursor for the production of CNFs. This comprehensive review presents the state-of-the-art of the manufacture of CNFs from lignin via the electrospinning technique. The first part of this review is concerned with the properties of lignin, the structure and applications of CNFs, especially for energy storage, and the description of the electrospinning method. The second part is focused on the different lignin-based precursor formulations for the manufacture of electrospun CNFs. These include the use of lignin alone or blended with other polymers at various mass ratios (polyacrylonitrile, poly(vinyl alcohol), poly(ethylene oxide), cellulose acetate, poly(ethylene terephthalate), and polyvinylpyrrolidone). In addition, different manufacturing approaches and strategies aiming to enhance the textural, mechanical, and electrochemical properties of CNFs are discussed in connection with their performance in relative applications.

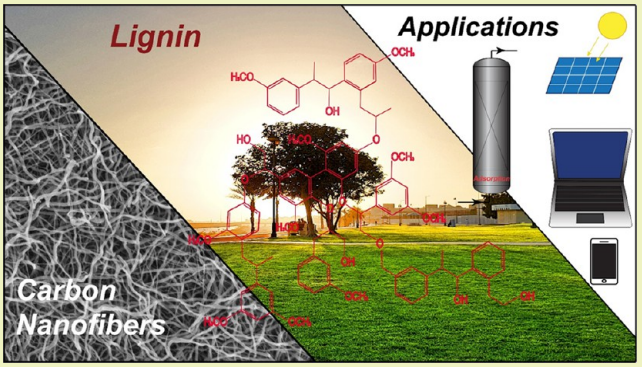


**KEYWORDS:** *Lignin, Carbon nanofibers, Electrospinning, Energy storage, Porous carbon, Electrochemical properties, Mechanical properties*



## INTRODUCTION

**Lignin.** Lignocellulosic biomass extracted from plants is considered to be the most promising biorenewable carbon-containing resource on earth. This biomass source consists of cellulose (35−83% dry weight basis), lignin (1−43% dry weight basis), and hemicellulose (0−30% dry weight basis). The relative content of each of these three components depends on the plant source.[1]

Lignin is the second most abundant natural polymer on Earth after cellulose, accounting for around 30% of the organic carbon existing in the biosphere, while it is the main biorenewable source of aromatic structures.[2,3] Its main function as a structural component in plants is to inhibit the diffusion of enzymes or solutions into the wood, rendering the cell walls stronger and more rigid.[1,4]

The structure of lignin is complex and amorphous, as it is highly branched.[2,4] It is constructed from the polymerization of three phenylpropane monomers (coniferyl, sinapyl, and *p*-coumaryl alcohols); inside the lignin structure these three units are termed as guaiacyl (G), syringyl (S), and *p*-hydroxyphenyl (H), respectively (Figure 1).[1,2] The configuration of the lignin structure differs according to the plant species, and it is also influenced by the environment. Generally, in softwoods (coniferous wood) the G units are prevalent; in hardwoods (deciduous trees) the amounts of G and S are almost equal and only traces of H are present, whereas in monocot grasses the ratio of the three monomers G/S/H is around 70/25/5.[1,4]

The extraction of lignin from the lignocellulosic biomass is industrially achieved through one of the following paper pulp processes, which aim at solubilizing lignin in order to obtain pure cellulose.

*Kraft Process.* This is the most widely used method (approximately 85% of the produced lignin is extracted with the kraft process).[2] It is performed at high temperatures (∼170 °C) and high pH values (∼13−14) in which lignin is dissolved in solutions of NaOH and $Na_2S$.[2,3] Kraft lignin contains small amounts of ash and sulfur, and it usually has a

Received: April 30, 2020
Revised: July 23, 2020
Published: August 17, 2020

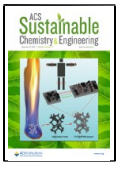





https://dx.doi.org/10.1021/acssuschemeng.0c03246
*ACS Sustainable Chem. Eng.* 2020, 8, 13868−13893

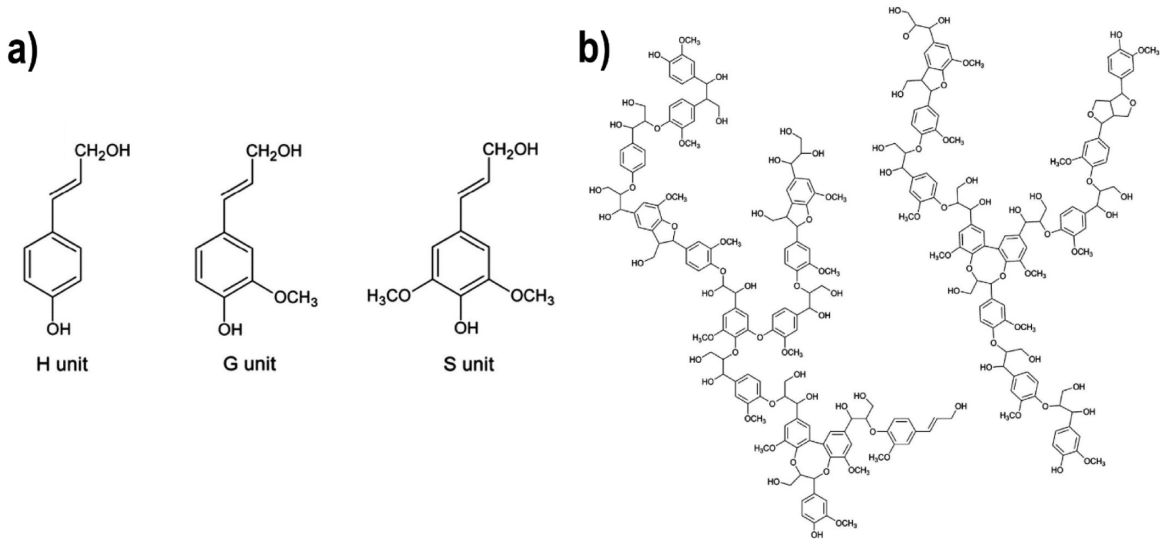


**Figure 1.** (a) Three lignin monomer units. (b) Typical structure of softwood lignin (Adapted with permission from ref 3. Copyright 2014 Elsevier).

molecular weight of around 1000−15 000 Da.[1,2] The ash can, however, be removed with proper chemical treatment.[5]

*Sulfite Process.* This method is very common in the pulp and paper industry.[2] It proceeds through the reaction of lignin with a metal sulfide and $SO_2$ at high temperatures (120−180 °C) for 1−5 h.[2] The lignosulfonates produced here are water-soluble; they contain a considerable amount of sulfur (4−8%) and ash, but also a higher molecular weight compared to kraft lignin (1000−50 000 Da).[1,2]

*Soda Process.* This process is applied to nonwood lignocellulosic biomass (grass, sugar cane, etc.).[2,3] It is similar to the Kraft process as the biomass is digested at high temperatures (140−170 °C) in NaOH solution in the presence of anthraquinone.[2] Soda lignins are sulfur-free and they have a range of molecular weight between 1000 and 3000 Da.[1,2]

*Organosolv Process.* This extraction method is based on the treatment of the lignocellulosic biomass with organic solvents (methanol, ethanol, acetic, and formic acid) mixed with water at high temperatures (170−190 °C) in the presence of catalysts. It produces sulfur-free, more pure lignin, with low ash content and low molecular weight (500−5000 Da). Disadvantages of this method include the corrosion of the equipment, the high cost of the solvents, and the presence of undesirable side reactions.[1−3] Alcell lignin is a type of organosolv lignin commercialized by Lignol Innovations.[6]

In addition to the above, lignin derived from the enzymatic hydrolysis of biomass has been reported[7] and also lignin extracted using organic solvents with ionic liquids.[8] The lignins produced from these processes have some structural differences which affect their physicochemical properties. Kraft and sulfite lignin contain sulfur (1−8 wt %) and ash (mainly salts of alkali metals), while soda and organosolv lignin are sulfur-free.[9] In terms of their solubility, sulfite lignin is soluble in water, while kraft lignin becomes water-soluble after sulfonation, as well.[2] Kraft and organosolv lignin are soluble in organic solvents, while soda lignin dissolves in alkaline solutions.[2,9] Moreover, sulfite lignin has the highest polydispersity index (6−8), while the other three types have polydispersity values between 1.5 and 3.5.[9] For the removal of impurities and ash in lignin, various methods can be applied such as acid treatment or cleaning with micro-organisms.[10]

The heterogeneous structure and the relatively high polydispersity are obstacles in the wider use of lignin. This can be overcome by filtration or selective precipitation to produce more homogeneous fractions; however, the large quantities of solvents needed are a disadvantage for the industrial scale-up.[3] These issues, together with its immiscibility with various polymer matrices and its poor mechanical properties, have rendered this significant biorenewable resource rather unexploited. It has been estimated, that out of 50−70 million tons of lignin extracted from the paper industry in 2010, only 2% was commercialized for applications such as adhesives, dispersants, antioxidants, and surfactants.[1] Most of the lignin produced is used as low-grade burning fuel or it is simply discarded as waste.[9]

Nevertheless, lignin can potentially emerge as a significant, versatile raw material through chemical modification. This includes amination, nitration, hydroxyalkylation, esterification and alkylation of its hydroxyl groups among others.[9] These processes can in turn lead to its use as a precursor for a wide range of products such as biodiesel, pharmaceutical precursors or polymers.[1,2,4] Without chemical modification, lignin is a very attractive precursor for the manufacture of carbon materials, such as carbon fibers and activated carbon. Its suitability for this purpose is based on its low cost, its large availability, the relatively high carbon content in its structure (around 60 wt %) and the absence of toxic byproducts during its thermal treatment.[11] The thermal decomposition of lignin during its conversion to carbon consists of multiple steps over a wide temperature range. Usually, there is an initial decomposition step between 150 and 275 °C (dehydration from hydroxyl groups), then the aliphatic chains start to break away from the aromatic rings at around 300 °C, at 370−400 °C carbon−carbon cleavages occur in the lignin backbone and, finally, at 500−700 °C the rearrangements in the lignin structure lead to char formation (mainly polyaromatic graphitic and disordered carbon).[1] During this process, volatile compounds are released, mainly $H_2$, $H_2O$, $CH_4$, CO, $CO_2$, and phenolic compounds.[12]



https://dx.doi.org/10.1021/acssuschemeng.0c03246
ACS Sustainable Chem. Eng. 2020, 8, 13868−13893

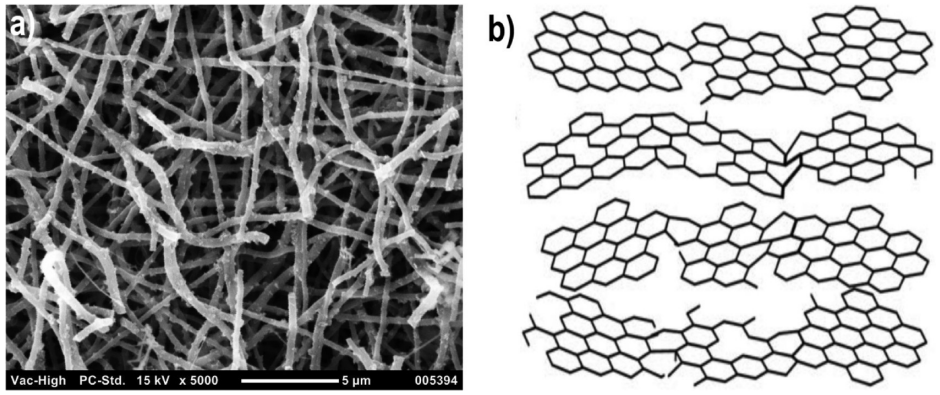


**Figure 2.** (a) SEM image of lignin-based electrospun CNFs (image taken by our research group, the scale bar is 5 $\mu$m). (b) Stacking of defective graphene layers constituting the structure of CNFs (Adapted with permission from ref 14. Copyright 2016 John Wiley and Sons).

**Carbon Nanofibers—Structure, Properties, and Applications.** *Morphology and Structure.* Carbon materials have revolutionized the materials science in the last few decades and they are projected to be at the forefront of emerging technological advances. Carbon nanofibers (CNFs), a one-dimensional form of carbon, belong to this class of materials, and they show a promising potential for a wide range of engineering applications. While conventional carbon fibers have typically diameters of few micrometers up to few tens of micrometers, CNFs have diameters in the range between few tens of nanometers up to submicron values. A strict definition would require the use of the prefix "nano-" for dimensions up to 100 nm, however, the term "nanofibers" is commonly encountered in the literature for fibers with diameters of up to few hundreds of nanometers (as mentioned, e.g., in ref 13); here, we will follow this convention. In applications where the surface area is important, lowering the average diameter to this range is highly beneficial.

The morphology of CNFs is characterized by a continuous network of long carbonaceous filaments which usually have a smaller or larger degree of interconnection (Figure 2a). Unlike carbon nanotubes (CNTs) which consist of perfectly wrapped concentric graphene layers, the structure of CNFs is more random, although it mainly consists of $sp^2$-hybridized carbon, as well.[13] Their structure comprises graphitic regions, which have a higher degree of order consisting of stacked graphene layers, and more disordered regions with randomly oriented defective graphene layers.[13,14] The degree of order depends on the method of production and the precursor materials.[13,15] The structure of CNFs is typically examined via X-ray diffraction (XRD) and Raman spectroscopy. The domains of disordered graphene layers in carbonaceous materials are sometimes termed as "turbostratic", although this term has been criticized (see ref 16 for a thorough discussion on this issue). Figure 2b presents a model for the stacking of defective graphene layers in the structure of carbon fibers (adapted from ref 14). These layers comprise regions which have a perfect hexagonal structure (the stacking of which builds the graphitic regions) and others in which the graphene layers are flawed (containing 5- or 7-carbon rings, open rings, etc.). These defects induce curvature which disrupts the parallel stacking of graphene layers, forming disordered regions resembling the shape of crumpled paper (see ref 17 for a detailed discussion about these structures). The disordered regions contain more unoccupied space, which translates into higher porosity.[17]

*Fabrication Methods.* CNFs are mainly fabricated using the following methods:

(a) *Chemical vapor deposition (CVD)*: According to this method, CNFs are produced from the decomposition of gaseous hydrocarbon precursors (such as $CH_4$, $C_2H_6$, $C_2H_2$, etc.) in the presence of metal catalysts inside a reactor.[13,15,18] This process is performed at high temperatures (700−1200 K).[13,15] The catalysts used in this case are metal nanoparticles consisting of Ni, Co, Fe, or various alloys.[13,15,18] As the gases are heated until they decompose, C atoms precipitate on the catalyst surface and develop graphitic filamentous structures.[13,15] Their diameter ranges from few tens to few hundreds of nanometers, while their length from less than a micron until few millimeters.[18] The shape of the graphitic structure (e.g., platelet-stacked or cup-stacked) is determined by the type of catalyst used.[15] The CNFs produced with this method have excellent thermal conductivities, however their production cost is rather high.[13]

(b) *Spinning*: Carbon fibers, with diameters higher than 5 $\mu$m, are traditionally fabricated from a polymeric precursor using a spinning technique, such as wet spinning, gel spinning, dry spinning or melt spinning.[13] In all these techniques, the precursor polymer is initially formed into fibers, followed by their thermal treatment at high temperatures (>600 °C) under inert atmosphere.[13,15,18] In the melt spinning technique, the precursor polymer is heated until it melts and then it is drawn through a spinneret for the formation of microfibers. In the other techniques, the polymer is dissolved in a suitable solvent and then it is ejected through a spinneret.[13] The fiber diameters are adjusted via the spinneret size and the drawing speed. Nevertheless, these techniques are not suitable for producing nanometer-sized carbon fibers. Instead, the most suitable method for this purpose is electrospinning, which is a variation of dry spinning. As CNFs are the main topic of this review, the electrospinning technique and the polymer precursors used for this purpose will be described in more detail in a separate section.

(c) *Other methods:* Template-based strategies and biomass methods have also been reported for the preparation of CNFs. These, however, are beyond the scope of this


https://dx.doi.org/10.1021/acssuschemeng.0c03246
ACS Sustainable Chem. Eng. 2020, 8, 13868−13893

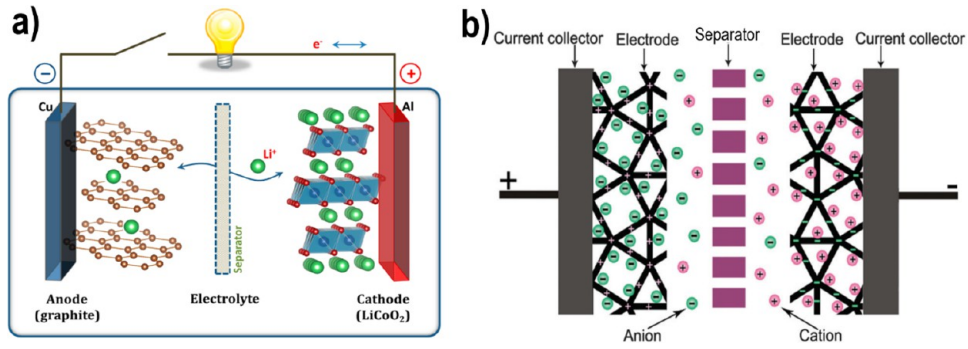


**Figure 3.** (a) Typical configuration of a lithium-ion battery (Reproduced from ref 22. Copyright 2013 American Chemical Society). (b) Typical configuration of a supercapacitor (Reproduced with permission from ref 28. Copyright 2016 Royal Society of Chemistry).

review; further information about them can be found in ref 15.

*Properties and Applications.* The main advantage of CNFs is their very small diameter which translates into a very high aspect ratio (their length/diameter ratio is typically more than a few hundreds) and into a very high surface area.[13] They can also be thermally or chemically treated in order to increase their porosity and their BET surface area to values as high as 2500 $m^2/g$.[13] Their large surface area can facilitate the doping with metals or metal oxides and, thus, enhance their applicability. Moreover, their surface can relatively easily be functionalized in order to introduce functional groups and alter their surface properties and their dispersion in various matrices.[13,19] CNFs possess good flexibility and mechanical strength depending on the degree of order of their microstructure, which in turn is dependent on the choice of the precursor and the fabrication method.[18] Their tensile strength can reach values of up to 4.8 GPa, which, however, is an order of magnitude less than that of carbon nanotubes, and also significantly lower than that of carbon microfibers produced through melt-spinning.[18,19] Their electrical conductivity can vary significantly from $10^{-7}$–$10^{3}$ S/cm.[13] Defects in their structure lower their crystallinity, but this can be advantageous in applications related to energy storage as their energy density is enhanced through higher charge storage in these defects.[13] Moreover, although they generally have lower thermal conductivity (<1600 W/(mK)) compared to carbon nanotubes (2000–6000 W/(mK)), they possess the advantages of easier dispersion and lower fabrication cost.[13,18]

Due to their high surface area, chemical resistance and thermal stability, CNFs have successfully been used in catalysis (catalyst support),[19] as adsorbents for the removal of sulfur impurities from fuels,[20] for air and water purification,[19] in biomedical applications, e.g. as templates for cell growth,[19] for polymer-based nanocomposites,[13,19] in dye-sensitized solar cells, and in sensors.[19] Their most common use, however, is in energy storage applications, particularly as electrodes for lithium-ion or sodium-ion batteries and for supercapacitors. Therefore, a brief description of these devices and the role of the CNFs in them will be presented in the following section.

*Energy Storage Applications.* Among escalating environmental concerns triggered by the consumption of fossil fuels, the shift toward the more widespread use of renewable energy is closely connected to the availability of efficient rechargeable batteries. Lithium-ion rechargeable batteries (LIB) are portable devices (electrochemical cells) that store and deliver electrical energy. Due to their unique characteristics (high energy density, safety, and relatively low cost), they are the basic power source for portable electronic devices.[21] Each LIB consists of two electrodes, the cathode and the anode, which are separated by an electrolyte (Figure 3a). Typically, the cathode consists of a lithium cobalt oxide, the anode consists of graphite, and the electrolytes are organic carbonates. The electrochemical performance of these devices depends mainly on the electrode materials.[21,22]

The development of electric vehicles (EVs) that are powered by rechargeable batteries is a game changer, as they can totally transform the quality of life in big cities. Currently, the available EVs in the market are powered by batteries which consist of thousands of LIB cells connected in series. However, these batteries suffer from disadvantages that compromise the competitiveness of EVs against the conventional internal combustion engine cars. Particularly, it has been found that 33% of consumers are worried about the driving range of these vehicles, that is, the distance that can be traveled on a fully charged battery before it needs a recharge.[23] This feature is closely connected to the energy density of batteries and to the capacity of electrodes, as a higher energy density is necessary for an increased driving range. Graphite, which is typically used as an anode material for LIBs, has a theoretical capacity of 372 mAh/g, and this limits the energy density of LIBs.[13,15] In contrast, significant capacities of more than 1000 mAh/g have been reported when nanometer-sized CNFs are used as anodes, because they comprise a large porosity for the accommodation of lithium ions.[13,15] Thus, CNFs can provide a possible solution to the limited energy density of LIBs.

The latest EVs available on the market (June 2020) have a satisfactory driving range of more than 300 miles (data from the U.S. Department of Energy[24]), but the charging time is another important issue, as it usually takes more than 8 h for a full charge. The nanostructured morphology of CNFs comprises a vast network of interfiber porosity that offers much higher ionic transport rates compared to the micrometer-sized graphite, in which the diffusion distance of $Li^+$ to and from its pores is very long.[15] Thus, the use of CNFs as an anode material can offer a faster charging time. Another important issue associated with the use of rechargeable batteries in EVs is that of cost. Although the price of LIBs has been constantly declining in the last 10 years, they are still estimated to cost around $114 per kWh (2020 price estimation by Forbes[25]), while Bloomberg projects their price to be $94 per kWh in 2024.[26] In the case of Tesla EVs, the current prices translate to an average battery cost of $9000



https://dx.doi.org/10.1021/acssuschemeng.0c03246
ACS Sustainable Chem. Eng. 2020, 8, 13868–13893

per car, which amounts to a significant 15% of the average vehicle price.[25] Here, the use of a renewable, low-cost precursor such as lignin can have a significant role in the manufacture of efficient CNF-based battery anodes that will cost less than the conventional graphite anodes. The use of CNFs as anode materials can also contribute to the production of more lightweight LIBs for EVs. The batteries currently used in electric cars have typically a mass of more than 200−300 kg, which makes them difficult to handle. CNFs are more lightweight than graphite due to their interfiber voids, so using them as anode materials can lead to the manufacture of lighter batteries with much higher energy density.

Li−Si and Li−Sn alloys have been reported to offer much higher capacities than graphite (4200 and 990 mAh/g, respectively).[21] The issue with these materials, however, is that they suffer from significant expansion and contraction during charge/discharge cycles, which break down the electrode. It has been proposed that the use of carbon materials can prevent this phenomenon, by preparing carbon-based nanocomposites with Si or Sn which can buffer the volume changes.[21] Hence, CNF-based anodes containing Si or Sn can offer an alternative solution for the manufacture of LIBs with high stability and large capacities.[13]

On the other hand, the use of CNFs in battery cathodes can increase the stability and the electrical conductivity of the electrode, but it has minor contribution to its capacity.[13,15] CNFs-$LiFePO_4$ composites have been successfully tested for this purpose.[13] These lithium-containing phosphates are examples of polyanion oxide cathodes that are less suitable for portable electronic devices and EVs due to their relatively low volumetric energy density.[27] Nevertheless, the polyanion oxide cathodes combined with carbon for increased structural integrity are suitable for grid storage of electricity that is produced from renewable sources (solar and wind energy).[27]

Sodium-ion batteries (SIBs) are similar to LIBs in terms of configuration and operation principles, the basic difference being the use of $Na^+$ as charge carriers. Although they offer lower energy densities and operating voltages than LIB, their basic advantage is the large availability of Na in nature and its very low cost compared to Li.[29] The current price (March 2020) for trona, from which sodium carbonate is produced is around $220/ton,[30] while the price of lithium carbonate (battery grade) reaches the value of $8000/ton.[31] However, Na ions are larger than Li ions (1.02 vs 0.76 Å, respectively).[32] Graphite does not intercalate $Na^+$ efficiently due to the narrow interlayer distances of its structure; therefore, it is unsuitable as an SIB anode material.[15,29] Porous CNFs, however, can serve this purpose successfully because their porosity can be tailored.[13,15] In this case, the pore size distribution is a crucial parameter.[15] Heteroatom doping or CNF-based composites give significant values of capacity for these devices (>500 mAh/g).[15] Thus, a proper selection of materials, considering also their cycle life and safety, can possibly achieve comparable electrochemical performance with the lithium-ion batteries. Hence, the use of CNFs in these devices can pave the way for the production of low-cost rechargeable batteries with efficient energy density.

Supercapacitors are energy storage devices that feature very high power density (>10 kW/kg), fast charge/discharge rates (few seconds), and very long lifetime (>$10^6$ cycles).[28,33] They are widely used in digital communication systems and electronic devices.[34] They consist of two electrodes built usually from the same material and immersed into an electrolyte (Figure 3b).[34] The charge accumulation in them is based on the electrosorption of electrolyte molecules on the electrode/electrolyte interface (electric double layer capacitors, EDLCs), while in pseudo-super-capacitors there is an additional occurrence of faradaic redox reactions.[28,33] Carbon materials (graphene, activated carbon, carbon nanotubes) are the most common materials used in their electrodes thanks to their chemical stability, nontoxicity, and simplicity of processing.[28,33]

In the supercapacitors the capacitance is proportional to the surface area of the electrode, (the electrode/electrolyte interface).[34] However, this surface area is not equivalent to the surface area of the carbon material measured e.g. through $N_2$ adsorption, because it is not 100% electrochemically accessible during its contact with the electrolyte.[28] Here, the porosity characteristics of the carbon material determine the performance of the supercapacitor. A large number of micropores increases the surface area and it boosts the energy density and the capacitance of the device.[35] On the other hand, the presence of mesopores is crucial for the fast ion transport, especially in the case of large electrolyte molecules, and this feature enhances the power capability of supercapacitors.[33,36] Moreover, these pore sizes can host pseudocapacitative species (conductive polymers, transition metal oxides) which significantly increase the energy performance of these devices.[28,33] Hence, lignin-based CNFs are appropriate for the manufacture of electrodes for supercapacitors because the adjustable porosity is one of their key features, while the interfiber voids facilitate ion transport. In any case, the optimal pore size depends on the electrolyte system and a controlled network of interconnected micro- and mesopores is preferable.[33]

In addition, the electrode material must have good electrical conductivity, while the presence of oxygen-containing functional groups and nitrogen doping is beneficial with regards to pseudocapacitance.[28] Just like all biomass precursors, lignin contains a significant amount of oxygen, some of which remains in the CNFs together with the oxygen added after chemical activation or post-treatment. It should be noted, however, that the very high porosity compromises the electrical conductivity, so, a balance should be kept.[35] Although CNFs generally do not possess high electrical conductivity compared to other materials like graphene or carbon nanotubes, their advantages lie in their large electrochemically accessible surface areas, their interfiber porosity which accelerates the transport of ions and the ease of doping or functionalization.[33] For CNFs, with or without doping with metal oxides, relatively high capacitance values (>300 F/g) have been reported.[13]

Recently, the manufacture of supercapacitors with unconventional mechanical properties has gained attention. In this regard, supercapacitors which are flexible, stretchable or compressible can pave the way for the development of advanced wearable electronics or artificial skin.[28] Hence, lignin-based flexible CNF mats offer a promising prospect for these energy storage devices.[37−40] Figure 4a presents flexible lignin-based CNFs prepared from kraft lignin/PVA with mass ratio 75/25, carbonized at 1000 °C with a measured specific capacitance of 241.4 F/g (at 5 mV/s) and energy density of 6.5 Wh/kg.[40] In Figure 4b, flexible CNF mats produced from kraft lignin/PVA with mass ratio 80/20 are folded and bended for 50 cycles without failure.[39]



https://dx.doi.org/10.1021/acssuschemeng.0c03246
ACS Sustainable Chem. Eng. 2020, 8, 13868−13893

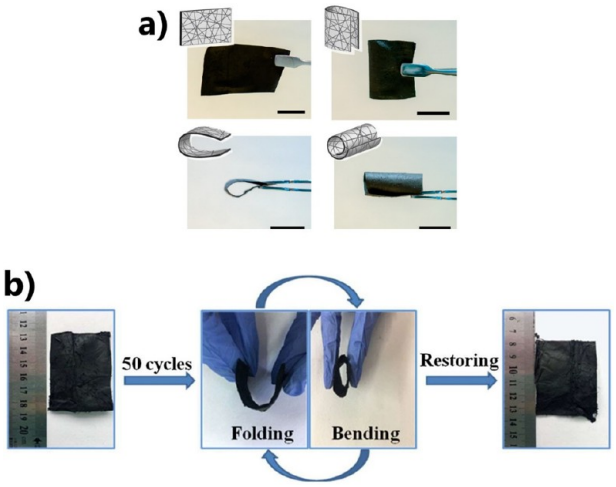


**Figure 4.** Examples of flexible lignin-based CNF mats. (a) Prepared from kraft lignin/PVA with mass ratio 75/25 (Reproduced from ref 40. Copyright 2020 American Chemical Society) and (b) prepared from Kraft lignin/PVA with a mass ratio 80/20 (Reproduced with permission from ref 39. Copyright 2018 Springer Nature). The scale bar in a is 15 mm.

**Electrospinning for CNF Manufacturing.** *Electrospinning Technique.* Electrospinning is a well-established technique for the fabrication of micro- and nanosized polymer fibers. Although it was first patented in 1934, it has received greater attention since the 1990s and it has also been applied at industrial level.[41]

In contrast to other fiber-spinning techniques such as melt spinning or dry spinning, which rely on mechanical forces to produce fibers by drawing the polymer through a spinneret, this technique relies on electrostatic forces.[41] A typical setup of the process is presented in Figure 5 (the setup can have

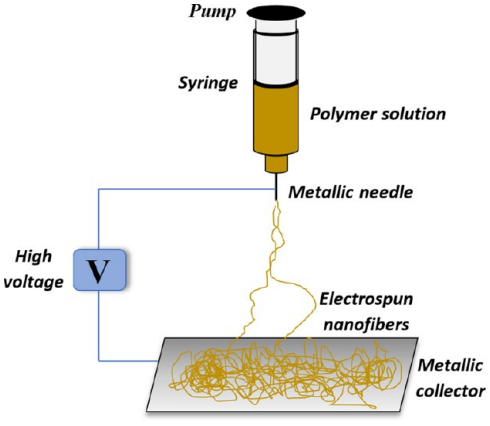


**Figure 5.** Typical electrospinning setup with vertical orientation.

either vertical or horizontal orientation). The polymer or the blend of polymers is initially dissolved into an appropriate solvent and loaded into a syringe which is connected to a pump offering a controlled flow rate. The metallic needle of the syringe is connected to a metallic collector through a high-voltage power supply. As the polymer solution is pumped through the needle, it is subjected to the electrostatic force from the electric field between the syringe and the collector. The shape of the pendant polymer droplet is, then, transformed into a cone (termed as the "Taylor cone"). When the electrostatic force overcomes the surface tension of the polymer solution, a jet is formed, which immediately breaks into a number of smaller jets. These jets follow looping trajectories and fall on the collector. During the ejection, the solvent evaporates and the jet is transformed into polymer fibers, which are usually solid and smooth.[42] In a typical setup, the fibers are randomly oriented and they form a nonwoven mat. However, variations of the collector allow the formation of aligned fibers (e.g., using a rotating drum).[13,42] Other variations of the setup allow the formation of core/shell structured fibers, in which the core polymer is different from the shell polymer, or hollow fibers.[13,42]

The fiber morphology is influenced by various process and material parameters. The most important of them are discussed in the following lines.

*Solution Concentration and Viscosity.* The solution concentration increases the solution viscosity, which in turns results in higher average fiber diameters.[13,41] When the concentration is below a certain point, the viscosity is too low, and then the jets breaks easily into droplets. In this case, many spherical beads form during the spinning, resulting in "beads-on-strings" morphology, or only beads (electrospray).[13,41] Therefore, a sufficiently high concentration is needed for bead-free fibers. At very high concentrations, however, the continuous flow is disrupted.

*Molecular Weight of the Polymer (Mw).* The longer the chain length, the higher is the molecular weight of the polymer.[41] This translates into more chain entanglements, resulting in higher average diameters and fewer beads.[41] When the polymer molecular weight is too low, then there is electrospray instead of fiber formation. This is a very usual case for lignin. Therefore, a high-Mw polymer (binder polymer) is added to the lignin solution to increase its spinnability.[43]

*Solvent Boiling Point.* A low boiling point is preferable for fast evaporation and dry fiber formation.[41] Nevertheless, a too volatile solvent can solidify in the needle and block it.[13] Moreover, the solvent evaporation affects the viscoelastic properties of the jet; fast evaporation results in a higher viscoelastic force, which in turn prevents the jet from stretching further. This produces fibers of larger diameters, as it has been reported in the case of polystyrene in tetrahydrofuran (boiling point 66 °C) vs polystyrene in dimethylformamide (boiling point 153 °C).[41]

*Surface Tension.* In most cases, it is better if the surface tension is kept rather low, so that a very high voltage is not necessary for the fiber formation.[13] Hence, the choice of solvent should be the appropriate one. Moreover, when the surface tension is low the formation of beads is avoided.[13] However, exceptions to this rule have been reported.[41]

*Electrical Conductivity.* It has been reported that the addition of salts into the solution produces finer, beadless fibers.[41] This is the result of higher elongational forces acting on the jet inside the electrostatic field.[41]

*Temperature.* This parameter influences the viscosity of the solution and the evaporation of the solvent. As an example, better spinnability of polyurethane fibers at relatively high temperature (70 °C) has been reported.[41] Nevertheless, there is no universal rule in this case.

*Humidity.* This is another important factor which affects the evaporation of the solvent. High humidity translates into slower evaporation, which in turn prevents the viscosity of the jet from increasing abruptly. On the other hand, high


https://dx.doi.org/10.1021/acssuschemeng.0c03246
ACS Sustainable Chem. Eng. 2020, 8, 13868−13893

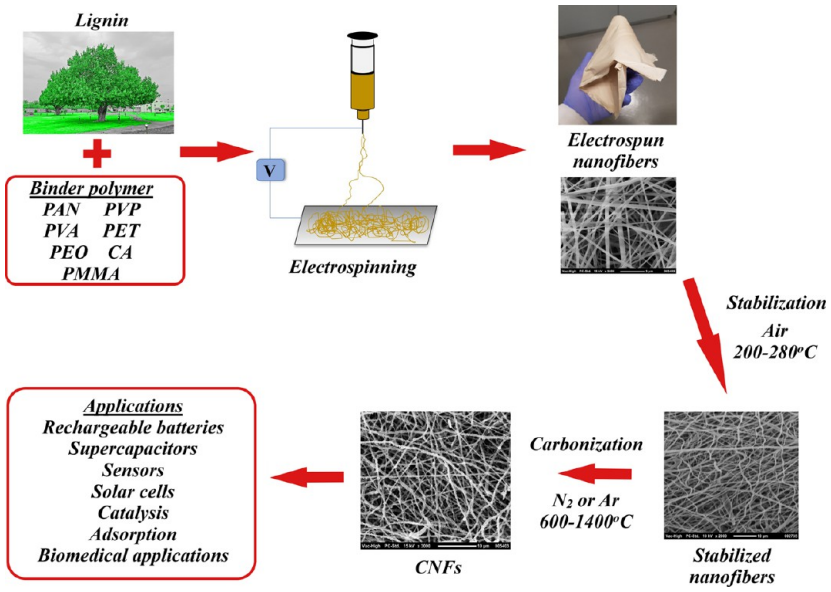


**Figure 6.** Methodology for producing CNFs from lignin using the electrospinning technique.

humidity can affect the charge density on the fiber surface.[41] Moreover, when more wet fibers are deposited on the collector, the slower evaporation can leave behind pores or a rough surface.[41]

*Applied Voltage.* The electrostatic force acting on the jet is influenced by the applied voltage. There is a voltage threshold above which the fiber formation is successful, and this depends on the surface tension and the viscosity of the solution.[13] In most cases a higher voltage results in thicker fibers.[41] The voltage, usually, varies between 15 and 30 kV.

*Spinning Distance.* Similar to the voltage, the spinning distance controls the electrostatic force. Here, the effect is not always clear; at a constant voltage, larger distance means weaker electrostatic field. However, in this case the jet has more time to stretch and dry.[41] Therefore, the effect is not always the same.

*Flow Rate.* Various reports have stated that larger fiber diameters are produced at higher flow rates, because of the speed with which the jet travels toward the collector.[13,41] At higher flow rates, higher voltage is required, as well.[13] The flow rate values for continuous fiber formation are, however, unique for each system.

There is a vast variety of more than 100 polymers which have been processed via electrospinning.[42] The popularity of this technique is justified by a number of advantages, such as its simple setup, the easiness in controlling the fibrous morphology by simply adjusting the process parameters and the huge variety of polymers or polymer blends that can be used. Furthermore, it is a versatile technique since interesting variations have been developed, e.g. different configurations for producing core/shell or hollow fibers, the production of composite fibers by incorporating micro- or nanosized fillers, multichannel structures, aligned fibers, or even the fabrication of ceramic fibers.[44,45] The most important drawbacks of this technique are the use of harmful solvents and sometimes the viability of scaling up at industrial level, especially when low concentrations or low flow rates have to be used. Electrospun nanofibers have been used in diverse applications including the manufacture of filters, in biomedical applications (tissue scaffolds), for sensors, in electrochemical applications (electrodes, photovoltaic devices, etc.), in controlled drug delivery, in protective clothing and as reinforcing fibers in composites.[41,43,45]

*Manufacturing of Electrospun-Based CNFs.* In addition to the applications mentioned in the previous section, electrospun nanofibers made of certain precursors are used for the fabrication of CNFs. Despite the variety of polymers processed via electrospinning, only a few of them have been used as precursors for the preparation of CNFs, that is, polyacrylonitrile (PAN), lignin, pitch, polyimide (PI), poly(vinylidene fluoride) (PVDF), poly(vinyl alcohol) (PVA), and more recently cellulose acetate.[13,44,46,47] The reason is that the precursor must satisfy some criteria in order to be carbonizable to CNFs. The most important is that it should not melt when heated at very high temperatures (above 800 °C) or, at least, that it can undergo some thermal or chemical treatment to become infusible during heating.[11] In this context, polymers containing heteroatoms (N, O, S, P, halogens), double bonds, and aromatic rings in their chains are more appropriate.[11] Furthermore, the polymer must dissolve into an electrospinning-appropriate solvent and it should give a considerable carbon yield. PAN is the most common polymeric precursor for CNFs because it gives a high carbon yield (>50%), and it produces CNFs with very good mechanical properties.[13] It can only be carbonized after it is first thermostabilized through heat treatment in air at 200−280 °C.

The general methodology for the manufacture of CNFs from lignin using the electrospinning technique is concisely depicted in Figure 6. Lignin-based electrospun CNFs were first reported in 2007, although the production of lignin-derived carbon microfibers using other methods had previously been reported.[48] In a previous section, it was mentioned that lignin has a relatively low molecular weight depending on its plant source and the method of extraction. Although a few research groups have reported the successful electrospinning of lignin alone and the carbonization into CNFs,[40−45] in most cases the electrospinning of lignin yields spray instead of fibers. Therefore, the presence of another polymer of higher Mw is necessary in the electrospinning


https://dx.doi.org/10.1021/acssuschemeng.0c03246
ACS Sustainable Chem. Eng. 2020, 8, 13868−13893

**Table 1. Lignin-Based Electrospun Carbon Micro- and Nanofibers: Literature Summary[a]**

| reference and purpose[b] | material parameters[c] | electrospinning parameters | thermal treatment[e] | average fiber diameter | porosity characteristics | properties of CNFs[f] | electrochemical performance[g] |
|---|---|---|---|---|---|---|---|
| | lignin type/solvent | voltage/distance | stabilization | electrospun | BET surface area | tensile str. | |
| | polymer mass ratio | flow rate | carbonization | carbonized | total pore volume | Y. modulus | |
| | additives | concentration[d] | activation | | meso-/microporous | conductivity | |
| 48 | organosolv/EtOH | 12 kV/20−25 cm | 0.25 °C/min, 200 °C, 24 h | 400−2000 nm | 1200 $m^2/g$ | - | - |
| properties | -/- | 0.5−1 mL/h | 10 °C/min, 900 °C | 200 nm | 0.484 $cm^3/g$ | - | - |
| | - | L/EtOH: 1/1 w/w | - | | microporous | - | - |
| 53 | organosolv/EtOH | 12 kV/20−25 cm | 0.05 °C/min, 200 °C, 36 h | 800−3000 nm | 505−1195 $m^2/g$ | - | - |
| properties | -/- | 0.8 mL/h | 10 °C/min, 600−1000 °C | 400−1000 nm | 0.233−0.523 $cm^3/g$ | - | - |
| | Pt-prec.: 0.2 and 0.4 wt % | L/EtOH: 1/1 w/w | - | | microporous | - | - |
| 50 | organosolv/EtOH | 14−22 kV/25 cm | 0.08 °C/min, 200 °C, 100 h | N/A | 747−1289 $m^2/g$ | - | - |
| catalysis | -/- | 1−3 mL/h | 10 °C/min, 900 °C | 600−3000 nm | 0.18−0.51 $cm^3/g$ | - | - |
| | $H_3PO_4$ 30 wt % | L/EtOH: 1/1 w/w | - | | meso- and micro- | - | - |
| | Pt-prec.: 0.6 and 3 wt % | | | | | | |
| 51 | organosolv/EtOH | 24 kV/30 cm | 0.08 °C/min, 200 °C, 6 h | 400−1000 nm | 850−2000 $m^2/g$ | 303 MPa | ED: 15−20 Wh/kg |
| catalysis | -/- | 3 mL/h | 10 °C/min, 900 °C | 400−1000 nm | 0.329−0.849 $cm^3/g$ | 4 GPa | (predicted) |
| electrodes | $H_3PO_4$ 30 wt % | L/EtOH: 1/1 w/w | $N_2/O_2$:97/3 v/v, 900 °C | | mostly microporous | - | - |
| 52 | organosolv/Ac/$CCl_4$ | 38 kV/13 cm | 2 °C/min, 250 °C, 1 h | 1300−5200 nm | 532−2447 $m^2/g$ | - | SC: 133 F/g (1 A/g) |
| supercapacitor | -/- | 0.2 mL/min | 1000 °C, 1 h | 1300−2500 nm | 0.28−1.58 $cm^3/g$ | - | ED: 42 Wh/kg |
| | hexamine 7.5−10% | 35 wt % | steam, 900 °C | | meso- and micro- | - | PD: 91 kW/kg |
| 49 | Kraft/DMF | N/A/13 cm | 0.5 °C/min, 250 °C, 15 min | 769 nm | 676−1204 $m^2/g$ | - | SC: 155 F/g (0.1 A/g) |
| supercapacitor | -/- | 1 mL/h | 3 °C/min, 900 °C, 30 min | 567 nm | 0.22−0.55 $cm^3/g$ | - | ED: 4 Wh/kg |
| | - | 50 wt % | $CO_2$, 600 °C, 1 h | | meso- and micro- | - | PD: 52 kW/kg |
| 56 | organosolv/EtOH | 0.4 kV/cm | 200 °C, 1 h | N/A | 840−2340 $m^2/g$ | - | SC: 48 F/g (2 A/g) |
| supercapacitor | -/- | 1−3 mL/h | 900 °C | 1−4 $\mu$m | 0.34−1.05 $cm^3/g$ | - | ED: 8.4 Wh/kg |
| | $H_3PO_4$/L: 1/10−3/10 | L/EtOH: 1/1 w/w | $O_2/N_2$: 0.5−6.5%, 900 °C | | microporous | - | PD: 47 kW/kg |
| 57 | lignosulfonate/DMF | 25 kV/20 cm | 250 °C, 1 h | 200−500 nm | ∼10−30 $m^2/g$ | - | Cap: 247 mAh/g |
| SIB | L/PAN: 10/90−50/50 | 1 mL/h | 800−1300 °C, 30 min | N/A | N/A | - | CD: 0.1 A/g |
| | - | 12 wt % (PAN) | - | | microporous | - | CS: 90.2%, 200 cycl. |
| 58 | N/A/DMF | 20 kV/15 cm | 250 °C, 3 h | N/A | 17.5−68.8 $m^2/g$ | - | Cap: 127.7 mAh/g |
| LIB | L/PAN: 50/50 | 1.5 mL/h | 1200 °C, 1 h | 150 nm | 0.026−0.081 $cm^3/g$ | - | CD: 5 A/h |
| | Pluronic P 123 | 12 wt % (PAN) | - | | mesoporous | - | - |
| 59 | Kraft/DMF | 19 kV/16 cm | 2 °C/min, 280 °C, 1 h | N/A | 2331−2543 $m^2/g$ | - | SC:128 F/g (1 A/g) |
| supercapacitor | L/PAN:10/90−30/70 | 0.8 mL/h | 5 °C/min, 1000 °C | 79−184 nm | Vmes, max: 0.955 $cm^3/g$ | - | ED: 59 Wh/kg |
| | - | 10 wt % | $CO_2$, 1000 °C, 1 h | | meso- and micro- | 530 S/m | - |
| 7 | EHL/DMF | 25 kV/15 cm | 1 °C/min, 250 °C, 1.5 h | N/A | 578−631 $m^2/g$ | - | SC: 192.5 F/g (1 A/g) |
| supercapacitor | L/PAN: 0/100−70/30 | 4.8 mL/h | 10 °C/min, 800 °C, 1 h | 172−421 nm | 0.25−0.27 $cm^3/g$ | - | N/A |
| | - | 12 wt % | - | | microporous | - | CS: 88.8%, 2000 cycl. |



https://dx.doi.org/10.1021/acssuschemeng.0c03246
ACS Sustainable Chem. Eng. 2020, 8, 13868−13893

**Table 1. continued**

| reference and purpose[b] | material parameters[c] | electrospinning parameters | thermal treatment[e] | average fiber diameter | porosity characteristics | properties of CNFs[f] | electrochemical performance[g] |
|---|---|---|---|---|---|---|---|
| | lignin type/solvent | voltage/distance | stabilization | electrospun | BET surface area | tensile str. | |
| | polymer mass ratio | flow rate | carbonization | carbonized | total pore volume | Y. modulus | |
| | additives | concentration[d] | activation | | meso-/microporous | conductivity | |
| 60 | N/A/DMF/THF | N/A | 280 °C, 1 h | 310−650 nm | 376−1194 $m^2/g$ | - | SC:165 F/g (1 $mA/cm^2$) |
| supercapacitor | L/PAN/pitch: 0.78/7/3 | N/A | 5 °C/min, 800 °C, 1 h | ∼370 nm | N/A | - | ED: 22 Wh/kg |
| | Zn-prec.: 0−10 wt % | N/A | - | | | - | CS: 94%, 3000 cycl. |
| 61 | Kraft/DMF | 8.5 kV/20 cm | 1 °C/min, 280 °C, 1 h | N/A | - | - | SC:1757 F/g (2 $mA/cm^2$) |
| supercapacitor | L/PAN: 20/80 and 50/50 | N/A | 5 °C/min, 1000 °C | 270−590 nm | - | - | - |
| | $NiCo_2O_4$: 1.59 $mg/cm^2$ | 12−18 wt % | - | doped: >800 nm | - | - | CS:138%, 5000 cycl. |
| 62 | EHL/DMF | 15 kV/15 cm | 0.5 °C/min, 260 °C, 3 h | N/A | 1008−2439 $m^2/g$ | - | SC:267.3F/g (1 A/g) |
| supercapacitor | L/PAN: 50/50 | 1 mL/min | 5 °C/min, 1400 °C, 1 h | N/A | 0.54−1.29 $cm^3/g$ | 2.82 GPa | ED: 9.28 Wh/kg |
| | graphene: 0−0.3 wt % | 20 wt % | KOH/CNFs: 6/1, 800 °C | | meso- and micro- | - | CS: 96.7%, 5000 cycl. |
| 63 | N/A/DMF | 24 kV/N/A | 1 °C/min, 225 °C, 2 h | 105−250 nm | - | - | - |
| sensor | L/PAN: 50/50−75/25 | 0.3 mL/h | 1200 °C | <100 nm | - | - | - |
| | graphene: 0−5 wt % | 10−20 wt % | - | | - | - | - |
| 54 | organosolv/DMF | N/A/10−15 cm | 200−275 °C, 1−12 h | 250−270 nm | - | - | - |
| thermoelectric generator | L/PAN: 0/100−70/30 | 10 μL/min | 900 or 1100 °C, 1 h | 130−150 nm | - | - | - |
| | - | 10−15 wt % | - | | - | 27.47 S/cm | - |
| 64 | Kraft/DMF | 16 kV/N/A | 10 °C/min, 250 °C | 283−412 nm | - | 160 GPa·$mm^3/g$ | - |
| properties | L/PAN: 10/90−30/70 | 0.8 μL/min | 1400 °C, 30 min | 185−253 nm | - | ∼14000 GPa·$mm^3/g$ | - |
| | copolymer 10−30 wt % | 10 wt % | - | | - | | - |
| 65 | N/A/DMF | 15 kV/12 cm | 200−280 °C, 2 h in total | 150−200 nm | - | - | - |
| properties | L/PAN: 50/50 | 0.04 mm/min | 600−1000 °C, 2−3 h | ∼100 nm | - | - | - |
| | | 12 wt % | - | | - | - | - |
| 66 | Kraft/DMF | 17 kV/20 cm | - | ∼3500 nm | - | - | - |
| properties | L/PAN: 50/50 | 0.03 mL/h | 1st step: 550 °C, 2 h, $H_2$ | ∼3500 nm | - | - | - |
| | cellulose nanofibrils | 17 wt % | 2nd step: 1000 °C, 1 h, Ar | | - | - | - |
| 67 | Kraft/DMF | 17 kV/25 cm | - | 1000−1200 nm | ∼15−31 $m^2/g$ | - | - |
| properties | L/PAN: 50/50 | 0.1 mL/h | 1st step: 550 °C, 2 h, $H_2$ | 615−989 nm | - | - | - |
| | Fe-, Pd-precursors | 15 wt % | 2nd step: 1000 °C, 1 h, Ar | | - | - | - |
| 68 | Kraft/DMF | 8.5−10 kV/15 cm | 10 °C/min, 250 °C, 2 h | N/A | - | 89.4 MPa | - |
| properties | L-g-PAN copolymer | 0.85−10.5 μL/min | 600−1400 °C, 30 min | 561−926 nm | - | 2.5 GPa | - |
| | - | 15−18 wt % | - | | - | 21.3 S/cm | - |
| 8 | EHL/IEL/DMSO/IL | 16−24 kV/10 cm | 1 °C/min, 250 °C, 2 h | 700−1200 nm | 536 $m^2/g$ | - | SC: 151 F/g (0.1 A/g) |
| supercapacitors | L/PAN: 100/0−0/100 | 0.5 mL/h | 2 °C/min, 800 °C, 2 h | 842 nm | 0.26 $cm^3/g$ | - | ED: 6.68 Wh/kg |
| | - | N/A | - | | meso- and micro- | - | CS: 95%, 20000 cycl. |
| 69 | N/A/DMF | 18 kV/10 cm | 250 °C, 1 h | 154−451 nm | 57−292 $m^2/g$ | - | - |
| adsorption | L/PAN: 10−50 wt % | 2 mL/h | 1000 °C, 1 h | ∼326 nm | 0.053−0.163 $cm^3/g$ | - | - |
| | - | 7.5 wt % (PAN) | $HNO_3$ treatment | | meso- and micro- | - | - |



https://dx.doi.org/10.1021/acssuschemeng.0c03246
ACS Sustainable Chem. Eng. 2020, 8, 13868−13893

**Table 1. continued**

| reference and purpose[b] | material parameters[c] | electrospinning parameters | thermal treatment[e] | average fiber diameter | porosity characteristics | properties of CNFs[f] | electrochemical performance[g] |
|---|---|---|---|---|---|---|---|
| | lignin type/solvent | voltage/distance | stabilization | electrospun | BET surface area | tensile str. | |
| | polymer mass ratio | flow rate | carbonization | carbonized | total pore volume | Y. modulus | |
| | additives | concentration[d] | activation | | meso-/microporous | conductivity | |
| 70 | EHL/DMF | 20 kV/25 cm | 1 °C/min, 250 °C | N/A | 689 $m^2/g$ | - | SC: 344.6 F/g (1 A/g) |
| supercapacitors | L/PAN: 60/40 | 15 mL/h | 10 °C/min, 800 °C, 1 h | 175−253 nm | 0.38 $cm^3/g$ | - | - |
| | - | 12 wt % | (air plasma modification) | | meso- and micro- | - | CS: 102%, 2000 cycl. |
| 71 | lignosulfonate/DMSO | 18.5 kV/N/A | 1 °C/min, 280 °C, 1 h | 160−336 nm | 94−389 $m^2/g$ | - | - |
| properties | L/PAN: 0−50 wt % | 1 mL/h | 5 °C, 800 °C, 1 h | N/A | 0.05−0.17 $cm^3/g$ | - | - |
| | - | 10 wt % | - | | meso- and micro- | - | - |
| 72 | lignin bio-oil/DMF | 10−25 kV/15−25 cm | 1 °C/min, 220 °C, 6 h | 137−812 nm | - | 32.76 MPa | - |
| properties | L/PAN: 100/0−0/100 | 0.5−2 mL/h | 4 °C, 1000 °C, 4 h | 165 nm | - | 4.78 GPa | - |
| | - | 15−25 wt % | - | | - | - | - |
| 36 | N/A/DMF | 20 kV/N/A | 280 °C, 1 h | 310−470 nm | 495−570 $m^2/g$ | - | SC: 212 F/g (1 mA/cm) |
| supercapacitors | L/PAN: 10/90 | N/A | 5 °C/min, 800−900 °C, 1 h | N/A | N/A | - | ED: 26.5 Wh/kg |
| | MnCl2 5 wt % | N/A | - | | meso- and micro- | - | PD: 400 W/kg |
| 73 | N/A/DMF | 15 kV/10 cm | 1 °C/min, 250 °C, 3 h | (submicron) | 6.3−12.9 $m^2/g$ | - | Cap.: 150 mAh/g |
| LIB | L/PAN: 0/100−50/50 | 0.02 mL/min | 10 °C/min, 1000 °C, 1 h | (submicron) | N/A | - | current: 8.5 C |
| | - | 12 wt % | - | | N/A | - | CS: ∼100%, 50 cycl. |
| 74 | organosolv/DMF | 10 kV/20 cm | 0.2−2 °C/min, 220 °C, 1 h | N/A | - | 89 MPa | - |
| properties | L/PAN: 50/50 | 1 mL/h | 4 °C/min, 1400 °C, 2 h | N/A | - | 5.3 GPa | - |
| | iodine vapor, 70 °C | 20 wt % | - | | - | - | - |
| 75 | organosolv/DMF | 15 kV/20 cm | 0.2 °C/min, 200 °C, 12 h | 1300−1800 nm | - | 83 MPa | - |
| properties | L/PAN: 30/70−70/30 | 5 μL/min | 5 °C/min, 1000 °C, 30 min | 1000−1100 nm | - | 6.1 GPa | - |
| | (butyration) | 20 wt % | - | | - | - | - |
| 76 | soda, Kraft/DMF | 15 kV/15 cm | 0.3 °C/min, 280 °C, 1 h | 273−701 nm | - | 142 MPa | - |
| properties | L/PAN: 0.25/1−1/0.75 | N/A | 3 °C/min, 1000 °C | 177−522 nm | - | 10 GPa | - |
| | - | 15 wt % | - | | - | - | - |
| 77 | Kraft/$H_2O$ | 26 kV/25 cm | stepwise, 220 °C, >24 h | ∼200 nm | 583 $m^2/g$ | - | - |
| adsorption | L/PVA: 70/30 | 1.2 mL/min | 5 °C/min, 1200 °C, 1 h | ∼200 nm | 0.29 $cm^3/g$ | - | - |
| | - | 12 wt % | - | | meso- and micro- | - | - |
| 78 | Kraft/$H_2O$ | 26 kV/25 cm | stepwise, 220 °C, >24 h | ∼200 nm | 583 $m^2/g$ | - | SC: 83.3 F/g (0.25 A/g) |
| supercapacitor | L/PVA: 70/30 | 1.2 mL/min | 5 °C/min, 1200 °C, 1 h | ∼200 nm | 0.29 $cm^3/g$ | - | ED: 84.3 Wh/kg |
| | $MnO_2$ nanowhiskers | 12 wt % | - | | meso- and micro- | - | CS: 92%, 1000 cycl. |
| 38 | Kraft/$H_2O$ | 26 kV/25 cm | stepwise, 220 °C, >24 h | ∼200 nm | 583 $m^2/g$ | - | Cap: 951 mAh/g |
| LIB | L/PVA: 70/30 | 1.2 mL/min | 5 °C/min, 1200 °C, 1 h | ∼200 nm | 0.29 $cm^3/g$ | - | CD: 50 mA/g |
| | $Fe_2O_3$: 22−45 wt % | 12 wt % | - | | meso- and micro- | - | CS: 715 mAh/g, 80 cycl. |
| 37 | Kraft/$H_2O$ | 26 kV/25 cm | stepwise, 220 °C, >24 h | ∼200 nm | 583 $m^2/g$ | - | SC: 64 F/g (400 mA/g) |



https://dx.doi.org/10.1021/acssuschemeng.0c03246
ACS Sustainable Chem. Eng. 2020, 8, 13868−13893

**Table 1. continued**

| reference and purpose[b] | material parameters[c] | electrospinning parameters | thermal treatment[e] | average fiber diameter | porosity characteristics | properties of CNFs[f] | electrochemical performance[g] |
|---|---|---|---|---|---|---|---|
| | lignin type/solvent | voltage/distance | stabilization | electrospun | BET surface area | tensile str. | |
| | polymer mass ratio | flow rate | carbonization | carbonized | total pore volume | Y. modulus | |
| | additives | concentration[d] | activation | | meso-/microporous | conductivity | |
| supercapacitor | L/PVA: 70/30−30/70 | 1.2 mL/min | 5 °C/min, 1200 °C, 1 h | ∼200 nm | 0.29 $cm^3/g$ | - | ED: 5.67 Wh/kg |
| | - | 12 wt % | - | | meso- and micro- | - | CS: 90%, 6000 cycl. |
| 79 | Kraft/$H_2O$ | 26 kV/25 cm | stepwise, 220 °C, >24 h | ∼200 nm | 583 $m^2/g$ | - | - |
| Electrocatalyst | L/PVA: 70/30 | 1.2 mL/min | 5 °C/min, 1200 °C, 1 h | ∼200 nm | 0.29 $cm^3/g$ | - | - |
| | Ag-prec.: 11−25 wt % | 12 wt % | - | | meso- and micro- | - | - |
| 80 | Kraft/$H_2O$ | 22 kV/20 cm | iodine, 100 °C, 12 h | ∼570−770 nm | 1049 $m^2/g$ | - | Cap: 272 mAh/g |
| LIB/SIB | L/PVA: 50/50 | 1 mL/h | 2 °C/min, 600 °C, 1 h | 514−875 nm | 0.49 $cm^3/g$ | - | (after 100 cycl.) |
| | KOH: 5 wt % | 15 wt % | - | | microporous | - | CD: 50 mA/g |
| 81 | Kraft/$H_2O$ | 20 kV/15 cm | 2 °C/min, 250 °C, 1 h | 210−600 nm | 1370−2170 $m^2/g$ | - | SC: 88 F/g (1 A/g) |
| supercapacitor | L/PVA: 90/10−75/25 | 0.8 mL/h | 5 °C/min, 1000 °C, 1 h | 166−220 nm | 0.36−0.53 $cm^3/g$ | - | ED: 38 Wh/kg |
| | - | 24 wt % | $CO_2$, 800 °C, 30 min | | meso- and micro- | - | CS: 87%, 1000 cycl. |
| 82 | Kraft/$H_2O$ | 17 kV/20 cm | 4 °C/min, 250 °C, 2 h | 148 nm | 1689−2005 $m^2/g$ | - | SC: 205 F/g |
| supercapacitor | L/PVA: 75/25 | 8−10 μL/min | 4 °C/min, 600 °C, 1 h | 148 nm | 0.60−0.71 $cm^3/g$ | - | N/A |
| | - | 17.4 wt % | KOH/CNFs: 1/1, 900 °C | | mesoporous | 386 S/m | CS: 83%, 1500 cycl. |
| 83 | Kraft/DMSO | 15−20 kV/20 cm | 2.5 °C/min, 250 °C, 1 h | 410−750 nm | - | 526.3 MPa | SC: < 7.73 F/g |
| microelectrode | L/PVA:100/0−50/50 | 0.5 mL/h | 550−1200 °C, 1 h | N/A | - | 26 GPa | N/A |
| | - | 30 wt % | - | | - | 21.9 S/cm | N/A |
| 39 | Kraft/$H_2O$ | 15−20 kV/20 cm | 5 °C/min, 250 °C, 1 h | N/A | 193−941 $m^2/g$ | - | - |
| DSSC | L/PVA:50/50−80/20 | 1 mL/h | 800−1500 °C, 1 h | 200−250 nm | 0.12−0.53 $cm^3/g$ | - | - |
| | - | 10−25 wt % | - | | meso- and micro- | 502 S/m | - |
| 84 | Kraft/$H_2O$/AcAcid | 18 kV/N/A | 200 °C, 3 h | N/A | 478−1147 $m^2/g$ | - | - |
| adsorption | L/PVA: 1/0.1 | 0.4 mL/h | 600−1000 °C, 1 h | N/A | 0.43−0.73 $cm^3/g$ | - | - |
| | - | 27.5 wt % | steam, KOH, nitrates | | meso- and micro- | - | - |
| 85 | Kraft/$H_2O$/AcAcid | 18 kV/N/A | 200 °C, 3 h | N/A | - | - | - |
| adsorption | L/PVA: 1/0.1 | 0.4 mL/h | 600−1000 °C, 1 h | N/A | - | - | - |
| | - | 27.5 wt % | KOH/CNFs: 3/1, 800 °C | | - | - | - |
| 86 | Kraft/$H_2O$/AcAcid | 18 kV/N/A | 200 °C, 36 h | N/A | 1466 $m^2/g$ | - | - |
| adsorption | L/PVA: 1/0.15 | 0.4 mL/h | 10 °C/min, 600 °C, 1.5 h | 700−1000 nm | 0.89 $cm^3/g$ | - | - |
| | $Fe_3O_4$: 1.25% w/v | 27.5 wt % | - | | meso- and micro- | - | - |
| 87 | Kraft/$H_2O$/AcAcid:13/87 | 20 kV/15 cm | 0.5 °C/min, 220 °C, 20 h | N/A | 273−385 $m^2/g$ | - | SC: 131 F/g (0.3 A/g) |
| supercapacitor | L/PVA: ∼96/4 | 0.5 mL/h | 5 °C/min, 800−1000 °C, 1 h | 920−1520 nm | 0.09−0.12 $cm^3/g$ | - | ED: 14.77 Wh/kg |
| | - | 25.5 wt % | $KMnO_4$ treatment | | meso- and micro- | - | PD: 135 W/kg |
| 40 | Kraft/$H_2O$ | 17 kV/20 cm | stepwise, 220 °C, 8 h | 182 nm | 797−1419 $m^2/g$ | - | SC: 241.4 F/g |
| supercapacitor | L/PVA: 75/25 | 0.5 mL/h | 800−1400 °C, 1 h | 100 nm | N/A | - | ED: 6.5 Wh/kg |
| | - | 20 wt % | - | | meso- and micro- | - | CS: 90%, 1050 cycl. |



https://dx.doi.org/10.1021/acssuschemeng.0c03246
ACS Sustainable Chem. Eng. 2020, 8, 13868−13893

**Table 1. continued**

| reference and purpose[b] | material parameters[c] | electrospinning parameters | thermal treatment[e] | average fiber diameter | porosity characteristics | properties of CNFs[f] | electrochemical performance[g] |
|---|---|---|---|---|---|---|---|
| | lignin type/solvent | voltage/distance | stabilization | electrospun | BET surface area | tensile str. | |
| | polymer mass ratio | flow rate | carbonization | carbonized | total pore volume | Y. modulus | |
| | additives | concentration[d] | activation | | meso-/microporous | conductivity | |
| 88 | N/A/$H_2O$/AcAcid | 22 kV/15 cm | 0.5 °C/min, 250 °C | N/A | 486−555 $m^2/g$ | - | - |
| sensors | L/PVA: 1/0.1 | 1 mL/h | 800 °C | ∼1000 nm | 0.22−0.36 $cm^3/g$ | - | - |
| | $ZnCl_2$: 1 wt % | 27.5 wt % | - | | meso- and micro- | - | - |
| 89 | organosolv/DMF | 25−30 kV/15−20 cm | 0.2 °C/min, 250 °C, 1 h | 400−600 nm | 281−401 $m^2/g$ | - | SC: 121.5 F/g (0.5 A/g) |
| supercapacitor | L/PEO: 90/10 | 0.4−1 mL/min | 3 °C/min, 900 °C, 1 h | 400−600 nm | 0.193−0.394 $cm^3/g$ | - | N/A |
| | Fe-prec.: 5−25 wt % | ∼42.8 wt % | - | | meso- and micro- | - | CS: 73%, 1000 cycl. |
| 90 | Kraft/DMF | 11−12 kV/17 cm | 5 °C/min, 250 °C, 1 h | 875 nm | 374−456 $m^2/g$ | 76.3 MPa | - |
| properties | L/PEO: 28/0.2 | 2 mL/h | 600−1000 °C, 1 h | 634 nm | N/A | 4.8 GPa | - |
| | - | 30 wt % | - | | N/A | 19.6 S/cm | - |
| 91 | Kraft/1 M NaOH | 19−25 kV/18−20 cm | - | 172−478 nm | ∼905−1249 $m^2/g$ | - | SC: 192 F/g (0.1 A/g) |
| supercapacitor | L/PEO: 1/0.14 | 1 mL/h | 3 °C/min, 800 °C, 2 h→ | 163−331 nm | 0.38−0.52 $cm^3/g$ | - | ED: 2245 $\mu$Wh/$cm^3$ |
| | $NaNO_3$: 10−50 mol % | 12 wt % | →(5% $H_2$ in $N_2$) | | meso- and micro- | - | CS: 92.5%, 6000 cycl. |
| 55 | Kraft/DMF | 20 kV/25 cm | 5 °C/min, 250 °C, 1 h | 300−1400 nm | - | - | - |
| properties | L/PEO: 99/1 | 0.01 mL/min | 10 °C/min, 1000 °C, 1 h | N/A | - | - | - |
| | - | 25−30 wt % | - | | - | 0.18 S/cm | - |
| 92 | organosolv, kraft/DMF | 20 kV/20 cm | 0.2 °C/min, 200 °C, 12 h | ∼1000−1100 nm | - | 15.58 MPa | - |
| properties | L/PEO: 95/5 | 0.5 mL/h | 5 °C/min, 1000 °C, 30 min | ∼900−1000 nm | - | 24.54 GPa | - |
| | - | 30 wt % | - | | - | - | - |
| 5 | Kraft/$H_2O$ | 10−15 kV/12−20 cm | - | N/A | 446−1444 $m^2/g$ | - | - |
| properties | L/PEO: 7.4/2.6−9/1 | 1 mL/h | 600−850 °C, 30 min | 100−500 nm | 0.18−0.55 $cm^3/g$ | - | - |
| | NaOH or KOH, ratio over L: 0.1/1−0.5/1 | 10−11.7 wt % | - | | meso- and micro- | - | - |
| 93 | Kraft/$H_2O$ | 10−15 kV/12−20 cm | - | - | 475−885 $m^2/g$ | - | - |
| properties | L/PEO: 9/1 | 1 mL/h | 600−900 °C, 30 min | 500−2000 nm | 0.75−0.90 $cm^3/g$ | - | - |
| | NaOH/L: 1/2 | 10 wt % | $H_2SO_4$, 110/150 °C, 20 h | | meso- and micro- | - | - |
| 94 | Kraft/DMF | V/D: 70 × $10^3$ V/m | 0.5−5 °C/min, 25 °C, 1 h | 809 nm | - | 0.0085 N/Tex | - |
| properties | L/PEO: 99/1 | 4.2 × $10^{-10}$ $m^3/s$ | 5 °C/min, 600−900 °C, 1 h | N/A | - | N/A | - |
| | - | 30 wt % | - | | - | 2.35 S/cm | - |
| 95 | Kraft/DMF | 17.5 kV/15 cm | 1 °C/min, 250 °C, 2 h | 667 nm | - | 51.25 MPa | - |
| properties | L/PEO: 30/1 | 0.1 mL/min | 5 °C/min, 1000 °C, 2 h | 474 nm | - | - | - |
| | Pd-precursor | N/A | - | | - | - | - |
| 96 | Kraft/$H_2O$ | 10−15 kV/12−20 cm | - | N/A | (same as ref 5) | - | SC: 344 F/g (1 A/g) |
| supercapacitor | L/PEO: 9/1 | 1 mL/h | 10 °C/min, 850 °C, 30 min | (submicron) | (same as ref 5) | - | ED: 8.1 Wh/kg |
| | NaOH/L: 0.3/1 or KOH/L: 0.5/1 | 10 wt % | - | | (same as ref 5) | - | CS: 96%, 5000 cycl. |
| 97 | Kraft/DMF | 25 kV/15 cm | 0.05 °C/min, 250 °C, 2 h | 555−660 nm | - | 47.5 MPa | - |
| properties | L/PEO: 96/4 | 20 $\mu$L/min | 10 °C/min, 800 °C, 2 h | 344−370 nm | - | 4.267 GPa | - |



https://dx.doi.org/10.1021/acssuschemeng.0c03246
ACS Sustainable Chem. Eng. 2020, 8, 13868−13893

**Table 1. continued**

| reference and purpose[b] | material parameters[c] | electrospinning parameters | thermal treatment[e] | average fiber diameter | porosity characteristics | properties of CNFs[f] | electrochemical performance[g] |
|---|---|---|---|---|---|---|---|
| | lignin type/solvent | voltage/distance | stabilization | electrospun | BET surface area | tensile str. | |
| | polymer mass ratio | flow rate | carbonization | carbonized | total pore volume | Y. modulus | |
| | additives | concentration[d] | activation | | meso-/microporous | conductivity | |
| | PZAA-CNT | 35 wt % | - | | - | - | - |
| 98 | organosolv/DMF | 20 kV/20 cm | - | N/A | - | - | - |
| catalysis | L/PEO: 95/5 | 1 mL/h | 5 °C/min, 600 °C | 207−235 nm | - | - | - |
| | $TiO_2$ 50 wt % | 30 wt % | - | | - | - | - |
| 99 | organosolv, Kraft/DMF | 7−9 kV/10 cm | 1 °C/min, 200 °C, 2 h | N/A | - | - | - |
| electrodes | L/PEO: 90/10 | 3 mL/min | 5 °C/min, 1000 °C, 1 h | ∼100−250 nm | - | - | - |
| | Ketjen black: 1 wt % | 20 wt % | - | | - | - | - |
| 100 | organosolv/DMF | 7 kV/10 cm | 1 °C/min, 200 °C, 2 h | ∼1000 nm | 381−473 $m^2/g$ | - | Cap: 576 mAh/g |
| LIB | L/PEO: ∼9/1 | 1 mL/h | 10 °C/min, 900 °C, 2 h | ∼500 nm | 0.28−0.31 $cm^3/g$ | - | CD: 30 mA/g |
| | N-doping (urea) | 24.2% w/v | - | | meso- and micro- | 12.24 S/cm | CS: 91.8%, 50 cycl. |
| 101 | organosolv/DMF | 30 kV/15 cm | 0.2 °C/min, 250 °C, 1 h | N/A | - | - | SC: 72.1 F/g (0.5 A/g) |
| supercapacitor | L/PEO: 95/5 | 0.1 mL/h | 10 °C/min, 900 °C, 1 h | 400−500 nm | - | - | N/A |
| | Fe-prec.: 1−25 wt % | 30 wt % | - | | - | - | CS: 107%, 1000 cycl. |
| 102 | Kraft/DMF | 20 kV/25 cm | 5 °C/min, 250 °C, 1 h | ∼550−750 nm | - | 33.7 MPa | - |
| properties | L/PEO: 99/1 | 0.01 mL/min | 800−1000 °C, 1 h | ∼300−550 nm | - | 8 GPa | - |
| | NC cellulose: 1−5 wt % | 25−30 wt % | - | | - | 35 S/cm | - |
| 103 | Kraft/DMF | 15 kV/15 cm | stepwise, 270 °C, 1 h | ∼500−1000 nm | - | - | - |
| sensors | L/PEO: 99/1 | 0.31 mL/h | 3 °C/min, 1000 °C, 1 h | ∼500−1000 nm | - | - | - |
| | - | 50 wt % | - | | - | - | - |
| 104 | organosolv/$H_2O$ | 20 kV/20 cm | - | 490 nm | 642 $m^2/g$ | - | SC: 180 F/g (1 A/g) |
| supercapacitor | L/PEO: 9/1 | 2 mL/h | 5 °C/min, 800 °C, 2 h | N/A | 0.312 $cm^3/g$ | - | ED: ∼10 Wh/kg |
| | 0.5 M NaOH | 12 wt % | NaOH at electrospinning | | meso- and micro- | - | PD: ∼50 kW/kg |
| 10 | Kraft/DMF | 50−70 kV/m/20 cm | 0.5 °C/min, 250 °C, 1 h | 543−1000 nm | - | 11.64 MPa | - |
| properties | L/PEO: 95/5−99.9/0.1 | 0.42 μL/s | 5 °C/min, 1000 °C, 1 h | 464−1000 nm | - | 2374 MPa | - |
| | - | 22−35 wt % | - | | - | - | - |
| 105 | N/A/DMF | 24 kV/30 cm | 250 °C, 2 h | ∼1500 nm | - | - | - |
| properties | LPF/PVP: 3/1 | 0.39 mL/h | 800 °C, 2 h | ∼1000 nm | - | - | - |
| | polymeric precursor | 30 wt % | - | | - | - | - |
| 106 | Kraft/DMF | 15 kV/15 cm | 150 °C (24 h) + 350 °C (4 h) | N/A | 600−1140 $m^2/g$ | - | SC: 248 F/g (0.2 A/g) |
| supercapacitor | L/PVP: 1/2 | 0.2 mL/h | 3 °C/min, 800 °C, 1 h | 100−200 nm | 0.283−0.627 $cm^3/g$ | - | N/A |
| | Mg-prec./L: 0.5/1−2/1 | 20 wt % | - | | meso- and micro- | - | CS: 97%, 1000 cycl. |
| 107 | organosolv/DMF | 24 kV/N/A | 1 °C/min, 300 °C | 210−310 nm | 164−659 $m^2/g$ | - | SC: 406 F/g (0.5 A/g) |
| supercapacitor | L/PMMA: 9/1−1/9 | 5.3 μL/min | 800 °C, 2 h | 125−200 nm | 0.15−0.56 $cm^3/g$ | - | ED: 11.5 Wh/kg |
| | PVP, $SnCl_2$ | N/A | HF/$HNO_3$: 1/1 | | mostly mesoporous | - | CS: 95%, 10000 cycl. |
| 108 | organosolv/Ac/DMAc | 16−18 kV/24 cm | 2 °C/min, 300 °C, 2 h | 400−500 nm | - | - | - |
| properties | L/CA: 1/1−4/1 | 0.7 mL/h | 2 °C/min, 600−1200 °C, 1 h | 200−300 nm | - | - | - |
| | iodine vapor, 100 °C | 30 wt % | - | | - | - | - |



https://dx.doi.org/10.1021/acssuschemeng.0c03246
ACS Sustainable Chem. Eng. 2020, 8, 13868−13893

**Table 1. continued**

| reference and purpose[b] | material parameters[c] | electrospinning parameters | thermal treatment[e] | average fiber diameter | porosity characteristics | properties of CNFs[f] | electrochemical performance[g] |
|---|---|---|---|---|---|---|---|
| | lignin type/solvent | voltage/distance | stabilization | electrospun | BET surface area | tensile str. | |
| | polymer mass ratio | flow rate | carbonization | carbonized | total pore volume | Y. modulus | |
| | additives | concentration[d] | activation | | meso-/microporous | conductivity | |
| 109 | N/A/DMF/Ac: 1/2 | 20 kV/18 cm | 0.4 °C/min, 220 °C, 12 h | 140–340 nm | 552–1061 $m^2/g$ | - | SC: 320.3 F/g (1 A/g) |
| supercapacitor | L/CA: 1/1 | 0.8 mL/h | 4 °C, 600 °C, 2 h | N/A | 0.29–0.57 $cm^3/g$ | - | ED: 30.2 Wh/kg |
| | epichlorohydrin 0–10 wt % | 25 wt % | - | | meso- and micro- | - | PD: 400 W/kg |
| 110 | Kraft/Ac/DCH:2/1 | 20 kV/20 cm | - | 500 nm | 541 $m^2/g$ | - | Cap: 340 mAh/g |
| SIB | L/CA: 1/1 | 0.75 mL/h | 2 °C/min, 1000 °C, 1 h | 300 nm | 0.27 $cm^3/g$ | - | (after 200 cycl.) |
| | - | 8 wt % | - | | N/A | - | CD: 50 mA/g |
| 12 | Kraft/TFA | 30 kV/7.7–20 cm | - | 80–781 nm | - | - | - |
| properties | L/PET: 50/50 | 0.1–1 mL/h | 5 °C/min, 600 °C, 1 h | 136–727 nm | - | - | - |
| | - | 9–32% w/v | - | | - | - | - |
| 43 | Kraft/TFA | 20–30 kV/7–20 cm | 2 °C/min, 260 °C, 1 h | 229–1473 nm | - | - | - |
| properties | L/PET: 50/50–80/20 | 0.1–2 mL/min | 3 °C/min, 1000 °C, 1 h | >155 nm | - | - | - |
| | - | 10–25% w/v | - | | - | - | - |
| 111 | Kraft/TFA | 30 kV/20 cm | - | ~80–400 nm | 72–288 $m^2/g$ | - | - |
| properties | L/PET: 50/50–90/10 | 0.1 μL/min | 5 °C/min, 800 °C, 1 h | >100 | 0.06–0.194 $cm^3/g$ | - | - |
| | - | 9–25% w/v | $CO_2$, 600 °C, 1 h | | meso- and micro- | - | - |

[a]N/A denotes that further details are not reported in the article. A dash "-" denotes that the specific measurement or procedure was not carried out. [b]The purpose of each article, classified in the following categories: properties (the characterization of CNFs without testing them for a particular application), supercapacitor, lithium-ion batteries (LIB), sodium-ion batteries (SIB), electrodes, sensor, adsorption, thermoelectric generator, catalysis. [c]Abbreviations: L lignin; prec precursor (e.g., Pt-precursor, Fe-precursor, etc.); EtOH ethanol; Ac acetone; $CCl_4$ carbon tetrachloride; DMF *N*,*N*-dimethylformamide; IL ionic liquid; IEL ionic liquid extracted lignin; HF hydrofluoric acid; PMMA poly(methyl methacrylate); AcAcid acetic acid; PAN polyacrylonitrile; EHL enzymatic hydrolysis lignin; THF tetrahydrofuran; PVA poly(vinyl alcohol); DMSO dimethyl sulfoxide; PEO poly(ethylene oxide); NC Cellulose nanocrystalline cellulose; PVP polyvinylpyrrolidone; LPF lignin–phenol–formaldehyde; CA cellulose acetate; DCH *N*,*N*-dimethylcyclohexylamine; DMAc *N*,*N*-dimethylacetamide; TFA trifluoroacetic acid; PET: poly(ethylene terephthalate); CNT carbon nanotubes; PZAA amine-terminated polyphosphazene. [d]Refers to total polymer concentration in the spinning solution, unless otherwise noted. [e]Described as heating at a *X* °C/min heating rate, up to *Y* °C temperature of treatment, hold for time *Z* at the *Y* temperature. [f]Tensile strength, Young's modulus, and electrical conductivity: only the maximum achieved values are reported here. [g]Abbreviations: ED energy density; SC specific capacitance; PD power density; Cap specific capacity; CD current density; CS cyclic stability; cycl cycles.

solutions. This is usually PAN, PVA, or PEO (poly(ethylene oxide)).

Moreover, in order to prevent the lignin-based electrospun mats from melting and losing their fibrous morphology, they are first subjected to a stabilization step. During this stage, the precursor nanofibers are heated at a very slow rate (usually <1 °C/min, depending on the lignin type) under oxidative atmosphere (air) until they reach temperatures between 200 and 280 °C, where they are kept for a few hours. Detailed stabilization and carbonization conditions for every lignin-based electrospun CNFs found in the literature is presented in Table 1. This process can be very time-consuming (sometimes lasting for days), and it is a drawback for industrial scale-up; however, the slow heating is necessary for effective diffusion of $O_2$ into the bulk of the fibers.[51] During this step, oxygen-containing functional groups (carbonyl, carboxyl, ester groups) are incorporated into the lignin macromolecules and cross-linking reactions take place.[48] This procedure raises the $T_g$ of lignin significantly and it prevents the fusion among the fibers.[48] It should be noted, however, that some degree of fusion among the fibers is desirable in many cases. Interconnected fibers exhibit better mechanical properties, increased electrical conductivity and enhanced performance in electrochemical applications.[54,55] In rare cases the stabilization can be totally omitted.[12,33]

After the fibers have been stabilized, they are carbonized for their transformation into CNFs. During this process, the nanofibers are heated under inert atmosphere ($N_2$ or Ar) until they reach a temperature between 600 and 1400 °C, where they are kept for ~1 h in most cases. Detailed carbonization conditions can be found in Table 1. Here, the fibers decompose slowly and release volatile products ($H_2$, $CH_4$, $H_2O$, CO, $CO_2$, phenolic compounds), while their structure is transformed into $sp^2$-hybridized carbon as described in a previous section. After the carbonization, a step of activation is optionally added, for increasing the porosity of CNFs. The activation can be either chemical (e.g., treatment with KOH or NaOH) or physical (heating under $CO_2$ or steam) (see Table 1).



https://dx.doi.org/10.1021/acssuschemeng.0c03246
ACS Sustainable Chem. Eng. 2020, 8, 13868–13893

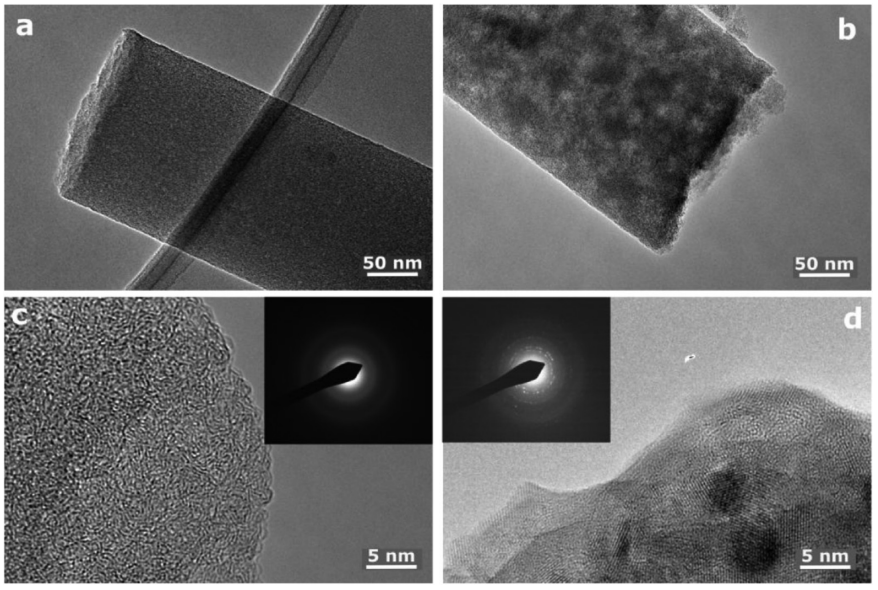


**Figure 7.** (a and c) TEM images of nonactivated lignin-based CNF prepared by Schlee et al.[49] (b and d) TEM images of the activated lignin-based CNF.[49] The diffraction pattern in d indicates the presence of polycrystalline graphite. The scale bars in a and b are 50 nm. The scale bars in a and b are 5 nm (Reproduced with permission from ref 49. Copyright 2019 Elsevier).

## LIGNIN-BASED PRECURSORS FOR CNF MANUFACTURING

Table 1 concisely presents a summary of the relevant literature focusing on the experimental conditions (material and electrospinning parameters, thermal treatment) and on some key properties of the CNFs (average diameters, porosity, mechanical, and electrochemical properties).

In the following sections, a more detailed account of the fabrication methodologies of CNFs is presented, focusing on the precursor formulation and on the CNF features arising from the preparation method.

**CNFs Prepared from Lignin Alone.** Lallave et al.[48] were the first to report the preparation of lignin-based electrospun CNFs. They used organosolv (alcell) lignin alone without any binder polymers, and they spun it into precursor fibers via coaxial electrospinning. The triaxial spinneret configuration consisted of (ethanol)/(lignin in ethanol)/(glycerine); the role of the outer ethanol sheath was to inhibit solidification, and the inner glycerine core acted as template fluid. After a lengthy stabilization step (24 h) which was necessary to prevent fusion, and the subsequent carbonization, highly microporous CNFs were produced with average diameters close to 200 nm. Their carbon content amounted to 94.3 wt %. The same research group elsewhere reported the production of carbon submicron-fibers doped with Pt.[53] The parameters of investigation here were the variation in carbonization temperature (600−1000 °C) and the presence of Pt. Increasing the treatment temperature resulted in a decrease of the average fiber diameter, higher carbon content (~95 wt % at 1000 °C), higher structural order, and increased porosity (reaching a BET surface area of 1195 $m^2/g$). The authors suggest that the high oxygen content in lignin functions as an activating agent for the development of porosity. The presence of Pt seemed to inhibit the structural ordering, while it did not affect significantly the growth of porosity. The preparation of Pt-doped CNFs from alcell lignin was further reported by the same research group in another article, in which the CNFs were tested as catalysts for the electro-oxidation of alcohols.[50] The difference, here, was the addition of $H_3PO_4$ in the spinning solution which functioned as activation agent for the enhancement of porosity and also as a stabilizing agent. Although phosphorus increased the electro-oxidation resistance of CNFs, it compromised their performance as electrocatalysts. Nevertheless, phosphorus-free CNFs containing well-dispersed Pt-nanoparticles with sizes of 2−3 nm performed very well in the electro-oxidation of methanol and ethanol.

You et al.[52] prepared organosolv lignin-CNFs using a different approach to improve the stabilization step. They added hexamine which decomposes to formaldehyde and acts as a cross-linker. Therefore, they could produce CNFs which retained their structural integrity. After steam activation, the CNFs exhibited a noteworthy BET surface area of 2447 $m^2/g$, and they contained a significant percentage of mesoporosity. Moreover, it was shown that a narrow micropore distribution is more effective than a large BET surface area in terms of the performance of CNFs as electrodes for EDLCs.

Schlee et al.[49] used kraft lignin (Mw: 1900 g/mol. Mn: 1200 g/mol) as CNF-precursor without the presence of any other binder polymers or additives. After activation with $CO_2$, the BET surface area of CNFs almost doubled from 676 to 1204 $m^2/g$, accompanied by a widening of pores and by an increase of the graphitic domains (Figure 7). The positive effect of pore widening was translated into an improved electrochemical performance in EDLCs, in which the activated CNFs performed better, having a specific capacitance of 155 F/g at 0.1 A/g and 113 F/g at 250 A/g, an energy density of 4 Wh/kg, and a power density of 52 kW/kg. The pseudocapacitance contribution of oxygen functional groups was also underlined.

**CNFs Prepared from Lignin/PAN.** PAN is very common as binder polymer for the fabrication of lignin-based CNFs due to its easy spinnability, its high molecular weight and the feasibility to be transformed into carbon fibers of relatively high mechanical strength.


https://dx.doi.org/10.1021/acssuschemeng.0c03246
ACS Sustainable Chem. Eng. 2020, 8, 13868−13893

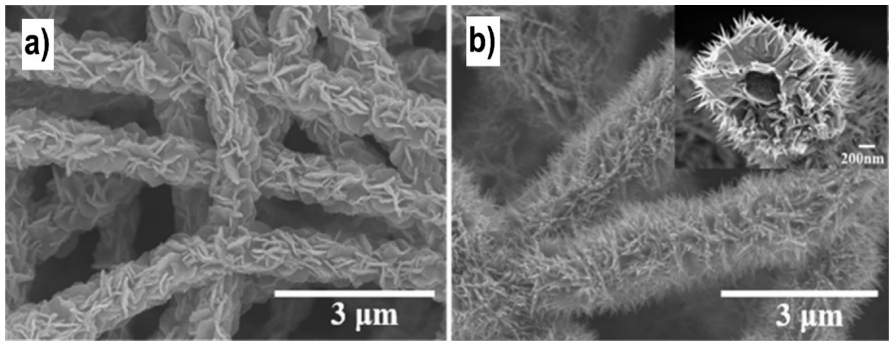


**Figure 8.** (a) $NiCo_2O_4$ nanosheets and (b) nanoneedles grown on lignin/PAN-based CNFs of different lignin content in the precursors [20 and 50 wt % respectively for a and b] (Reproduced with permission from ref 61. Copyright 2017 Elsevier).

Lignin/PAN-based electrospun CNFs have been commonly used as anodes for rechargeable batteries. Choi et al.[73] combined PAN with lignin at mass ratios ranging from 0/100 to 50/50 (lignin/PAN). They observed that increasing the lignin content resulted in thinner fibers with lower BET surface area, probably due to some fusion between them and lower Coulombic efficiency when tested as anodes for LIB. In contrast, Jin et al.[57] report better electrochemical performance of lignin/PAN CNFs when lignin content increases, and a very good overall cycling stability (247 mAh/g, over 200 cycles at 0.1 A/g) when tested as anodes for SIB. They attribute this result to the more defective carbon structure created at lignin/PAN mass ratio of 50/50, as it provides more sites for ion adsorption. The same research group further tested lignin/PAN-based electrospun CNFs as anodes for LIB.[58] The presence of a triblock copolymer which promoted mesoporosity and also some fusion among the fibers resulted in a satisfactory capacity (127.7 mAh/g) at a high current density of 5 A/g with a discharge time of 91 s.

Besides anodes for rechargeable batteries, lignin/PAN-based CNFs have also been applied as supercapacitor electrodes. Perera Jayawickramage et al.[59] blended Kraft lignin with PAN at mass ratios ranging from 10/90 to 70/30 respectively. The fibers containing the highest lignin percentage had the minimum average diameter (79 nm), the highest BET surface area (2543 $m^2/g$), the most ordered structure, and the highest electrical conductivity (530 S/m). Wang et al.[7] have also shown the positive effect of increasing lignin content (up to 60 wt %) in lowering the average diameter and increasing the BET surface area of lignin/PAN CNFs.

The doping of CNFs with metal-oxide nanoparticles or with heteroatoms is another strategy to increase their suitability for supercapacitor electrodes, by taking advantage of pseudocapacitive effects. With ZnO being a promising electrode material for supercapacitors, Yun et al.[60] fabricated ZnO-doped CNFs from a PAN/lignin/pitch precursor. Pitch, in this case, was added as a low-cost carbon source with higher electrical conductivity than PAN, while the oxygen-rich lignin promoted the development of porosity. In the absence of Zn, the CNFs were microporous (480 $m^2/g$), while the presence of zinc acetate boosted the porosity up to the value of 1194 $m^2/g$ for 5 wt % Zn, creating a meso/microporous texture. Owing to pseudocapacitive effects, the presence of ZnO was found to augment the electrochemical performance of the CNFs, reaching a specific capacitance value of 165 F/g at current density of 1 $mA/cm^2$ and a power density of 22 Wh/kg. Another doping method has been reported through the hydrothermal deposition of $NiCo_2O_4$ on lignin/PAN based CNFs,[61] which was achieved by dispersing the CNFs and the metal precursors in ethanol. Here, the metal oxides formed nanosheet-like and nanoneedle hierarchical structures which grew axially on the surface of the fibers (Figure 8).

For a 50 wt % lignin content in the precursor blend, the $NiCo_2O_4$-doped CNFs exhibited a very high specific capacitance of 1757 F/g at a current density of 2 $mA/cm^2$ which was more than an order of magnitude larger than that of undoped CNFs (46 F/g), combined with high energy density (47.75 Wh/kg) and power density (799.53 W/kg). Zhang et al.[70] applied post-treatment of CNFs with air plasma, which increased their oxygen and nitrogen content and enhanced their supercapacitor performance due to faradaic reactions. These fibers exhibited a specific capacitance of 344.6 F/g (at 1 A/g) which was almost double the capacitance of undoped CNFs (174.3 F/g).

Dai et al.[62] implemented another reinforcement strategy, as they added graphene nanosheets in the electrospinning solutions. Interestingly, it was found that the lignin/PAN-based CNFs doped with 0.3 wt % graphene had around 5 times higher N- and S-content than the undoped ones, probably because it retained some of the amount of $NH_3$ and $SO_2$ released from the polymers during carbonization. Moreover, the presence of graphene prompted a large increase in the BET surface area (2439 $m^2/g$), together with higher Young's modulus (2.82 GPa), higher degree of graphitization, and lower hydrophobicity.

Mustafov et al.[63] report the doping of CNFs with graphene as well, which lowered the degree of crystallinity of the electrospun nanofibers, but it increased the degree of graphitization and the electrical conductivity of CNFs. Here, CNFs of average diameter lower than 100 nm were produced.

Another potential energy-related application associated with CNFs is that of thermoelectric generators. Dalton et al.[54] studied the thermoelectric properties of lignin/PAN-based CNFs, by measuring their Seebeck coefficient, which is defined as the voltage difference generated by the sample when a temperature gradient is applied on it. The results showed that increasing the lignin content to 70 wt % induced a high degree of fusion among the fibers which built an interconnected CNF network and boosted their electrical conductivity (27.47 S/cm) and their Seebeck coefficient (10 $\mu$V/K).

Promoting the fusion and the interconnection among the fibers was the goal of Ding et al.[75] who esterified lignin with butyric anhydride. The butyration had a plasticizing effect as it transformed the hydroxyl groups of lignin into butyl esters, and, therefore, the $T_g$ of lignin decreased due to a higher


https://dx.doi.org/10.1021/acssuschemeng.0c03246
ACS Sustainable Chem. Eng. 2020, 8, 13868−13893

molecular thermal mobility. The morphology of the manufactured CNFs displayed a moderate interfiber bonding without losing their fibrous structure. As a result, the tensile strength of butyrated-lignin/PAN CNFs almost quadrupled compared to that of plain-lignin/PAN-based CNFs (83 vs 22 MPa).

As it was shown by Zhang et al.,[76] the lignin extraction process yields lignins of varying structural features, and it determines the mechanical properties of the CNFs. Soda lignin presented a more linear structure compared to kraft lignin, which was more complex and comprised many more polar functional groups. As a result, upon blending with PAN and processing for CNF preparation, the soda lignin-derived CNFs had a less defective structure and exhibited much higher tensile strength (142 MPa) than kraft lignin-based CNFs (99 MPa).

Another important feature demonstrated by the blends of lignin with PAN is their flexibility to be modified in order to improve various properties of the CNFs. Park et al.[64] added a lignin-grafted-PAN copolymer (30 wt %) as compatibilizer between these two raw materials. This modification increased the specific tensile strength of the CNFs to around 160 GPa·$mm^3/g$ and their Young's modulus to around 14 000 GPa·$mm^3/g$. Elsewhere, the same research group has reported the preparation of electrospun CNFs using as a precursor the lignin-grafted-PAN copolymer alone.[68] In this case, a tensile strength of 89.4 MPa was reported. The enhancement of mechanical properties was also the subject of study for Dai et al.,[74] who treated the precursor fibers with iodine vapor prior to the stabilization step. Iodine is known to form charge transfer complexes with aromatic rings. Introducing it into the precursor fibers allowed them to be stabilized at a relatively high heating rate (2 °C/min), therefore, more rigid CNFs with less structural defects and higher degree of graphitization were produced. Here, their tensile strength amounted to 89 MPa and their Young's modulus to 5.3 GPa.

Xu et al.[67] prepared Fe- and Pd-doped lignin/PAN nanofibers by adding the appropriate precursors in the electrospinning solution. After the fabrication of the CNFs, the presence of catalysts promoted the growth of carbon nanotubes on their surface through a chemical vapor deposition process (Figure 9). The CNT-grown CNFs exhibited high thermal stability (98.3% residual weight at 950 °C) due to their more graphitic structure, a super-hydrophobic character because of the hierarchical nanostructures grown on their surface, and increased BET surface area (31.45 vs 5.74 $m^2/g$ of the undecorated CNFs). Moreover, the same research group has reported the preparation of porous CNFs through coaxial electrospinning, in which the lignin/PAN solution formed the shell of the precursor fibers and acetylated cellulose-nanofibrils the core.[66]

**CNFs Prepared from Lignin/PVA.** PVA is also very often combined with lignin for the preparation of electrospun CNFs. Although it gives a very low carbon yield when treated at elevated temperatures (<10 wt %), it is soluble in water; therefore, it has high processability and the use of toxic solvents can be avoided. Moreover, similarly to lignin, the oxygen atoms in its macromolecule contribute to the development of microporosity.[77]

Prof. Hao Fong's group has reported in various articles the fabrication of lignin/PVA-based electrospun CNFs and their applications in adsorption, catalysis, and energy storage.[71−75] Starting from a 70/30 lignin/PVA mass ratio, the precursor

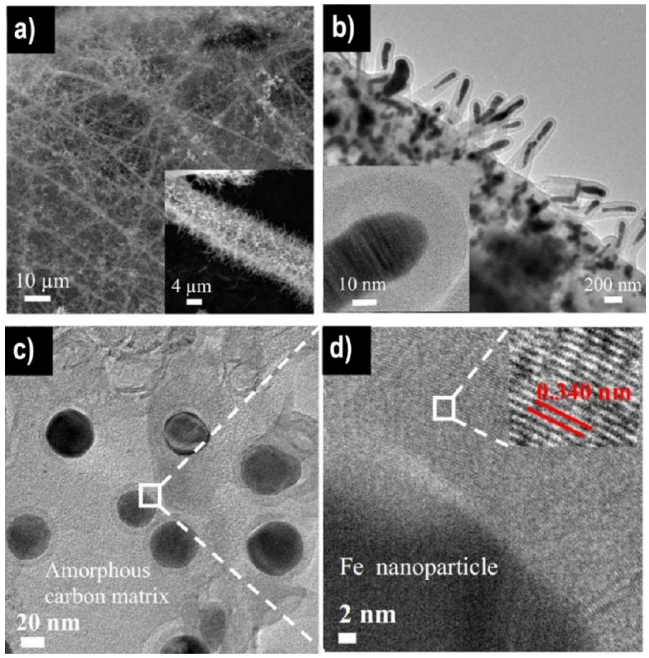


**Figure 9.** Carbon nanotubes grown on (a and b) Pd-doped; (c and d) Fe-doped lignin/PAN-based CNFs. The red marks in d measure an interlayer spacing of 0.340 nm (Reproduced with permission from ref 67. Copyright 2014 Elsevier).

electrospun fibers are initially subjected to a lengthy stabilization step (>24 h) prior to carbonization. The CNFs have average diameters of less than 200 nm, and they possess a significant BET surface area of 583 $m^2/g$ with an average pore size of 3.5 nm. These fibers were applied as adsorbents for the removal of methylene blue and tannic acid from aqueous solutions.[77] Comparing with commercial activated carbon of higher BET surface area (964 $m^2/g$), the CNFs exhibited almost 9-times higher adsorption capacity for methylene blue and 3.5 times higher adsorption capacity for tannic acid, accompanied by faster adsorption kinetics. The key property here was the relatively large average pore size, which posed less restrictions to the internal diffusion of the adsorbates into the adsorbent pores.

In order to improve their electrochemical performance, they were surface-decorated with varied amounts of $MnO_2$ nanowhiskers after treatment with $KMnO_4$ (Figure 10).[78] Here, it was found that the mats containing a moderate amount of $MnO_2$ (mass ratio of CNF/$MnO_2$: 1/1) displayed a specific capacitance of 83.3 F/g, which was much higher than that of undecorated CNFs (4.5 F/g) at 250 mA/g. A further increase in the amount of $MnO_2$ (mass ratio of CNFs/$MNO_2$: 1/2) induced a decrease in specific capacitance (25.8 F/g) and in cyclic stability. In addition, the research group tested the lignin/PVA-derived CNFs as electrocatalysts for the oxygen reduction reaction in alkaline fuel cells, after they doped them with Ag.[79] The deposition took place through the supercritical $CO_2$ method, after which Ag-nanoparticles sized ∼2−10 nm were uniformly deposited on the fiber surface. For CNFs loaded with 15 wt % Ag, their electrocatalytic activity was higher than that of a commercial Pt/C catalyst, recording a mass activity of 119 mA/mg. Further, the CNFs were doped with $F_2O_3$, which is known to possess a high theoretical capacity (1007 mAh/g).[38] The electrochemical measurements revealed that the CNFs containing 35 wt % $Fe_2O_3$


https://dx.doi.org/10.1021/acssuschemeng.0c03246
ACS Sustainable Chem. Eng. 2020, 8, 13868−13893

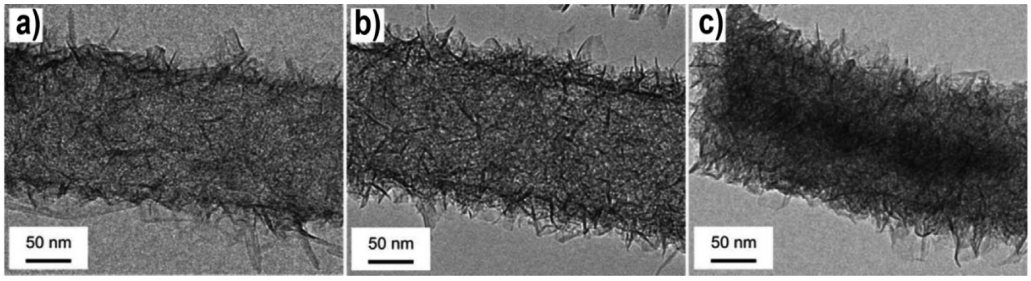


**Figure 10.** TEM images showing $MnO_2$ nanowhiskers grown on lignin/PVA based CNFs. The mass ratios between CNFs and $MnO_2$ in a, b, and c are 2/1, 1/1, and 1/2, respectively (Reproduced with permission from ref 78. Copyright 2016 Elsevier).

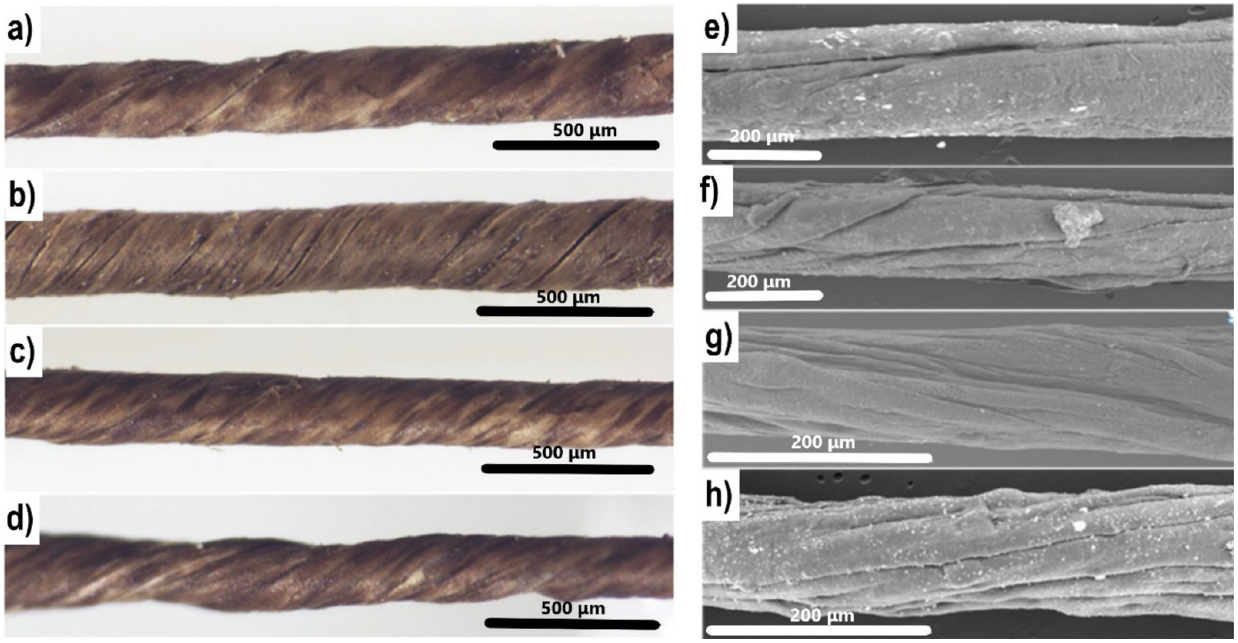


**Figure 11.** Optical images of twisted lignin/PVA electrospun fibers with (a) 23, (b) 44, (c) 54, and (d) 78 turns per cm (scale bar is 500 $\mu$m). (e–h) SEM images of the corresponding CNFs (scale bar is 200 $\mu$m) (Reproduced with permission from ref 83. Copyright 2019 Elsevier).

nanoparticles showed a remarkable specific capacity of 715 mAh/g after 80 cycles, reflecting a good electronic conductivity and superior lithium permeability. Undoped lignin/PVA-based CNFs activated with KOH have elsewhere exhibited a BET surface area of 1049 $m^2/g$ and a capacity value of 272 mAh/g (at 50 mA/g) after 100 cycles.[80]

Various other articles describe the utilization of lignin/PVA electrospun CNFs in energy-related applications (supercapacitors, LIB, dye-sensitized solar cells). Perera Jayawickramage et al.[81] have reported the fabrication of mesoporous CNFs from a lignin/PVA blend of mass ratio ranging between 90/10 and 75/25. After activation with $CO_2$, the average fiber diameter dropped significantly from around 600 nm to less than 200 nm, mainly due to the decomposition of PVA. At 20 wt % PVA content, the activated CNFs exhibited a very large BET surface area of 2170 $m^2/g$. The role of PVA as a porosity-generating template has also been highlighted in the work of Ago et al.[82] Here, the authors report that at 75/25 mass ratio between lignin and PVA, the PVA spontaneously segregates during electrospinning, producing precursor fibers with microphase separation. As PVA evolves into gas during carbonization, it acts as a sacrificial polymer inside the lignin scaffold. After activation with KOH, the CNFs possessed a high BET surface area (2005 $m^2/g$) of mesoporous texture, and they were used as free-standing working electrodes in supercapacitors. Their specific capacitance amounted to 205 F/g, with a capacity retention of 83% after 1500 cycles. As a means to boost their mechanical and electrical properties, a twisted CNF yarn morphology has been elsewhere suggested, which can be fabricated after the electrospinning step using a rotating motor assembly (Figure 11).[83] In this case, a gradual twisting of the CNFs induced a gradual increase in mechanical properties and in electrical conductivity but a gradual decrease in the specific capacitance because of the elimination of intefiber voids and the decreased porosity. The highly twisted fibers (Figure 11d) exhibited a tensile strength of 526.3 MPa, an electrical conductivity of 21.9 S/cm, and a specific capacitance of 0.0252 F/g, while the untwisted CNF mat had a tensile strength of 48.5 MPa, an electrical conductivity of 8.4 S/cm, and a specific capacitance of 7.73 F/g.

This twisted form enhanced the tensile strength of the CNFs by an order of magnitude (526.3 MPa vs 48.5 MPa of the untwisted mat) and their electrical conductivity significantly (21.9 vs 8.4 S/cm). However, their specific capacitance dropped considerably (by more than 20 times) compared to the untwisted mat, because the twist produced more compact yarns and eliminated the voids among the fibers which are crucial for the ion transport.



https://dx.doi.org/10.1021/acssuschemeng.0c03246
ACS Sustainable Chem. Eng. 2020, 8, 13868–13893

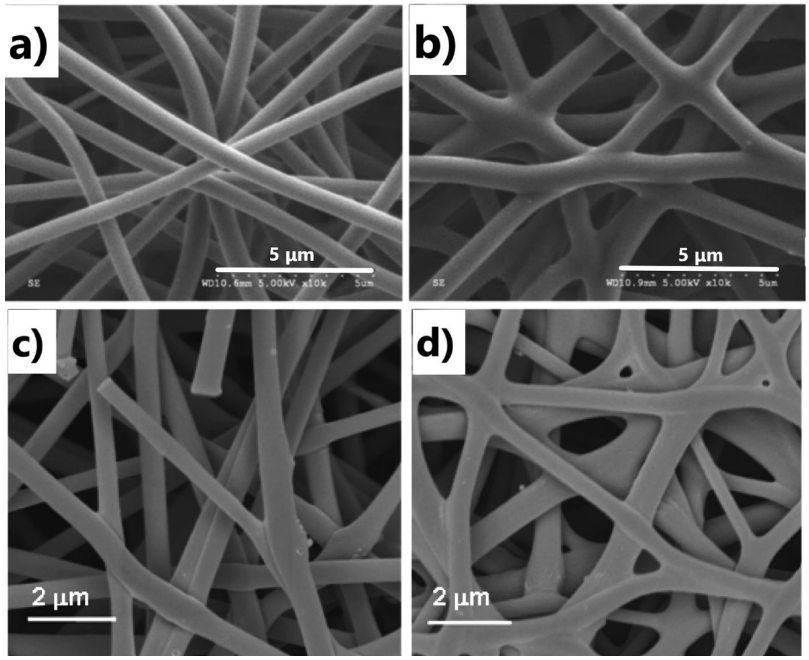


**Figure 12.** Examples of controlling the degree of fusion in lignin/PEO-based CNFs. (a and b) Different degrees of fusion induced by using different fractions of kraft lignin and the same amount of PEO (30 wt %);[90] in a a methanol/methylene chloride-soluble fraction of lignin is used and in b a methanol-soluble fraction of lignin is used (Adapted with permission from ref 90. Copyright 2013 John Wiley and Sons). (c and d) Different degrees of fusion induced by using different amounts of PEO and the same lignin precursor:[100] (c) 3 and (d) 10 wt % PEO (Adapted from ref 100. Copyright 2013 American Chemical Society). Scale bar: 5 $\mu$m in a and b; 2 $\mu$m in c and d.

On the other hand, Zhao et al.[39] focused more on the positive impact of the carbonization temperature on the electric properties of the CNFs. Raising the temperature to 1500 °C produced mesoporous CNFs with 941 $m^2/g$ BET surface area, which boosted their electrical conductivity (502 vs 212 S/cm for CNFs carbonized at 1000 °C) due to a higher degree of graphitization. These fibers were tested as binder-free counter electrodes of dye-sensitized solar cells, and exhibited a conversion efficiency of 7.60%, a value which is very close to that of a conventional Pt electrode.

Moreover, lignin/PVA-derived CNFs have been employed as adsorbents of high surface area. Meng et al.[85] have studied the adsorption of volatile organic compounds (toluene, methanol, acetone) in the gas phase on a bed of activated CNFs. The activation process was performed through treatment with KOH, which altered the surface chemistry of the fibers by incorporating oxygen functionalities. It was found that the nonpolar toluene adsorbed to a larger extent through physical and chemical adsorption, and the lactone groups had a positive contribution in that. On the other hand, the more polar acetone and methanol showed a preference for adsorption on more polar sites. The same research group has further reported the enhancement of porosity through doping with $Fe_3O_4$.[86] The presence of the metal oxide promoted the development of micropores in the CNFs and boosted their BET surface area (1466 $m^2/g$).

**CNFs Prepared from Lignin/PEO.** Small amounts of PEO (usually 1−10 wt %) are often added to lignin to improve its spinnability. PEO forms hydrogen bonds with the hydroxyl groups of the lignin macromolecules; studies have shown that these interactions are dependent on the type of lignin (softwood/hardwood).[112] Hence, it provides the necessary chain entanglements that facilitate electrospinning, while it does not interfere with the transformation of lignin to carbon.[5]

Shi et al.[92] have reported the blending of lignin with PEO in mass ratios of 95/5 respectively, in order to study the carbonization behavior of three different types of lignin, namely, ethanol-organosolv lignin, formic acid/acetic acid-organosolv lignin, and kraft lignin, named after their extraction method. It was found that the ethanol-organosolv lignin had a very low molecular weight, and it could not be thermo-stabilized as it melted. Similar results about this type of lignin have been reported elsewhere.[99] On the other hand, formic acid/acetic acid-organosolv lignin contains many side-chains; thus, it yielded defective carbon fibers with poor mechanical properties. Kraft lignin, in contrast, produced smooth, compact fibers with a higher degree of graphitization and a tensile strength of 15.58 MPa, because its macromolecules have better orientation and fewer side-chains. Elsewhere, it has been reported that lignin with a rather linear structure produced highly amorphous CNFs, while cross-linked lignin extracted from a different source produced CNFs with a higher graphitic content.[103] Vivo-Vilches et al.[99] have further reported that phosphoric acid-lignin gives CNFs of higher mechanical stability than kraft lignin, due to its larger Mw and its higher purity.

The difference in the stabilization behavior depending on the type of lignin has also been highlighted by Cho et al.,[55] who state that softwood kraft lignin can be stabilized at much faster heating rates (5−15 °C/min) than the hardwood organosolv lignins (often ∼0.1 °C/min). Although the stabilization step aims at preventing the melting and the collapse of the fibrous structure, the authors, here, stress the positive impact of a small degree of fusion in applications requiring mechanical stability. As the outer surface of the fibers softens, some "spot-welding" can be developed at


https://dx.doi.org/10.1021/acssuschemeng.0c03246
ACS Sustainable Chem. Eng. 2020, 8, 13868−13893

junctions with other fibers. Following cross-linking reactions that take place during stabilization, these spots can act as strengthening knots that increase the tensile strength and the elastic resilience of the carbon nanofibrous mats.

Moreover, the same research group has reported that this phenomenon boosts the electrical conductivity of the CNFs, as well, through facilitation of the electron transport.[102] Similar conclusions were drawn by Dallmeyer et al.[90] who measured improved tensile strength and electrical conductivity when interconnection between CNFs occurred (Figure 12a and b). Here, the interconnection of fibers was achieved by using different fractions of kraft lignin as precursors. The fraction which was soluble in methanol/methylene chloride produced infusible CNFs, while the fraction soluble in methanol produced interconnected CNFs. The interconnected CNFs exhibited improved mechanical properties and electrical conductivity compared to the infusible ones (tensile strength of 74.1 vs 32 MPa and electrical conductivity of 19.6 vs 2.3 S/cm, respectively).

On the other hand, Wang et al.[100] controlled the degree of fusion by incorporating the appropriate amount of PEO in kraft lignin (Figure 12c and d). In Figure 12c, the ratio of lignin/PEO is 97/3 and there is negligible fusion among CNFs; in Figure, 12d, this ratio is 90/10 and a considerable degree of fusion is apparent. In this case, the fused CNFs exhibited an increased charge capacity compared to the infusible ones (445 and 365 mAh/g, respectively, at 30 mA/g current density). Therefore, the role of PEO in controlling the interconnection between the fibers is pivotal. In their case, the electrical conductivity was further increased to 12.24 S/cm after nitrogen doping via treatment with urea, while a specific capacity of 576 mAh/g (at 30 mA/g current density) was measured upon application in LIB.[100] In addition, the conductivity of the CNFs has been shown to depend on the carbonization temperature, as the treatment at 900 vs 600 °C was found to increase the conductivity by 7 orders of magnitude due to the formation of a more ordered structure.[94] This observation agrees with other studies.[39]

The reinforcement with carbon nanotubes (CNTs) has been proposed as another method for improving the mechanical properties of CNFs.[97] In this case, the addition of a small amount (1 wt %) of CNTs functionalized with amine-terminated polyphosphazene in the electrospinning solution of lignin/PEO improved the tensile strength of CNFs by 53.2% (reaching 47.5 MPa) and their Young's modulus by 43.9% (reaching 4.26 GPa).

Adding alkali hydroxides in the electrospinning solution can increase the porosity of CNFs as activation occurs simultaneously with carbonization.[5,93,104] Hu et al.[5,93] added NaOH or KOH at different ratios (10−50 wt % per lignin weight) in the electrospinning solutions. This quantity of alkali hydroxides is significantly smaller (only 0.1−0.25%) compared to the quantity usually needed when a postcarbonization treatment is performed for fiber activation. Here, meso-/microporous CNFs were produced with a BET surface area of approximately 1400 $m^2/g$.[5] These fibers exhibited a specific capacitance of 344 F/g with 96% cyclic stability after 5000 cycles.[96] Additional treatment with concentrated $H_2SO_4$ at 110−150 °C for 20 h and hydrothermal treatment (water at 150 °C, 5 atm for 24 h) caused fragmentation of the CNFs and widening of the pores, but it decreased the microporosity and the BET surface area (752−885 $m^2/g$).[93] However, this treatment anchored sulfonic acid on the surface of CNFs, which were successfully applied in the hydrolysis of cellulose to glucose and nanocellulose.

Doping with Fe was applied by Wang et al.[101] and Yu et al.[89] to lignin/PEO precursors of 90/10 mass ratio in order to utilize the CNFs as supercapacitor electrodes. Adding moderate amounts of Fe-acetylacetonate precursor (~20−25% per polymer mass) enhanced the electrochemical performance of CNFs in supercapacitors via the contribution of redox faradaic reactions; the specific capacitance in these cases amounted to 72.1−121.5 F/g. Another doping strategy has been reported through the coating of the CNF surface with Pd via electroless plating, although no specific application was tested here.[95] Schlee et al.,[91] on the other hand, added an oxidizing agent ($NaNO_3$) in the electrospinning solution which already contained NaOH. Without any stabilization, the fibers were directly carbonized in a reducing atmosphere (5% $H_2$ in $N_2$ at 800 °C). The presence of $NaNO_3$ decreased the average fiber diameter by more than 50% compared to the undoped fibers (478 vs 200 nm). Furthermore, this oxidizing salt enhanced the microporosity and anchored oxygen functionalities which contributed to pseudocapacitative effects. Hence, the gravimetric capacitance amounted to 192 F/g (at 0.1 A/g) and the volumetric energy density to 2245 $\mu Wh/cm^3$.

**CNFs Prepared from Lignin Blended with Other Polymers.** Besides PAN, PVA, and PEO, which are the most common binder polymers for the electrospinning of lignin, a few other polymers have been successfully used for this purpose, each one contributing different features in the electrospun and in the carbonized fibers.

Jia et al.[110] blended kraft lignin with cellulose acetate at a 50/50 mass ratio. Cellulose acetate (CA) is the acetylated form of cellulose, which is an abundant, renewable, natural polymer like lignin. Hence, the production of CNFs in this case is totally based on natural precursors. Electrospun CNFs based on CA alone have been reported, as well.[113] An important issue that is associated with the use of this polymer for CNF preparation is that it must undergo deacetylation prior to carbonization to prevent its melting; this involves the treatment with a strong base, usually NaOH. The authors, however, report that after electrospinning, they proceeded directly to carbonization, without stabilization, which in this case was not necessary, probably due to the presence of lignin. The carbon fibrous structure, that they obtained, exhibited some fusion in the intersection of the fibers. This 3D interconnected network was employed as electrode in SIB and it displayed a specific capacity of 340 mAh/g at 50 mA/g after 200 cycles. An additive such as epichlorohydrin can be added to the spinning solution to enhance the interactions between lignin and CA.[109] Furthermore, Schreiber et al.[108] started from lignin/CA of different mass ratios (1/1−4/1, respectively), but stabilized the electrospun fibers initially with iodine vapor, and afterward with heating in air at 300 °C before carbonizing them. Iodine adsorbed in the lignin domains and helped stabilize the morphology, while the increasing lignin content resulted in a more disordered carbon structure.

Apart from CA, polyvinylpyrrolidone (PVP) can also be used as a spinning agent for lignin. Although PVP gives a low carbon yield after carbonization, it can be dissolved in various solvents, so, it functions as a scaffold for the development of porosity after its thermal decomposition. Ma et al.[106] used a blend of lignin/PVP with 1:2 mass ratio respectively to produce Mg-doped mesoporous CNFs with a BET surface


https://dx.doi.org/10.1021/acssuschemeng.0c03246
ACS Sustainable Chem. Eng. 2020, 8, 13868−13893

area of 1140 $m^2/g$. Furthermore, lignin has been blended with poly(methyl methacrylate) (PMMA) which also acts as sacrificial polymer;[107] using a co-electrospinning setup, core−shell mesoporous CNF structures were produced in this case.

Finally, lignin was recently combined with recycled poly(ethylene terephthalate) (PET) for the manufacture of electrospun CNF precursors.[12,43] Their blending and processing via electrospinning enabled the preparation of CNFs with average diameters ranging between 100 and 500 nm, depending on the lignin/PET mass ratio (50/50−90/10) and on the solution concentration (10−25% w/v). While the precursor fibers were carbonized without stabilization due to the amorphous nature of lignin, it was found that the degree of fusion and interconnection among the fibers depends on the lignin/PET mass ratio and on the average fiber diameter of the precursors. Hence at a high mass ratio (90/10), CNFs with an average diameter close to 100 nm and minimum fusion among them can be produced.[111] In contrast, at 50/50 mass ratio the mats consisting of very thin fibers (<200 nm) melt extensively, while the electrospun mats of larger average fiber diameters (~400 nm) remain infusible. This phenomenon was explained on the basis of varying decomposition rates, which are influenced by heat and mass transfer limitations.[12] In addition, $N_2$ physisorption measurements showed that the fusion between the fibers compromises the BET surface area, while PET acts as a sacrificial, porosity-developing template.[111]

## CONCLUSIONS AND FUTURE OUTLOOK

In this detailed review, the state-of-the-art of lignin-derived electrospun CNFs is summarized, highlighting the connection among the precursor formulations, the manufacturing strategies, the structure of the produced CNFs, and the properties that they carry for specific applications. Probably the most important feature of lignin-based CNFs is the variety of manufacturing strategies including the choice and the mass ratios of the precursors, the additives, the conditions of thermal treatment, and the feasibility of post-treatment. Based on the previous sections, a number of conclusions can be drawn:

(i) Although a few articles describe the manufacture of electrospun CNFs from lignin alone, the usual case is the addition of a binder polymer that promotes the electrospinnability of lignin.

(ii) Each of the binder polymers carries different features. PAN contributes to better mechanical properties; PVA can be electrospun using nontoxic solvents; PEO contains oxygen which is beneficial for the stabilization, and it can also control the degree of fusion among fibers; CA is derived from an abundant bioresource (cellulose), thus, 100% biobased CNFs can be produced from lignin/CA; PMMA, PVP, and PET act as sacrificial polymers for the development of porosity.

(iii) The electrospinning technique is suitable for minimizing the average fiber diameter and for controlling the morphology of CNFs. However, the use of organic solvents is an issue of consideration. Moreover, when low flow rates or low solution concentrations are required, the mass production of CNFs may not be viable.

(iv) Using the electrospinning technique, CNFs with average diameters of as low as 100−200 nm can be easily manufactured. Lowering the average fiber diameter at these levels minimizes the mass transfer limitations when the CNFs are used as adsorbents, catalyst supports, or electrodes.

(v) The porosity of CNFs can be customized through physical or chemical activation and with a careful adjustment of the process conditions. BET surface areas with values higher than 1000 $m^2/g$ are very common.

(vi) The structure and the purity of lignin vary depending on its plant source and on the method of extraction and these, in turn, influence the properties of CNFs. In general, kraft lignin can be stabilized faster than organosolv lignin, but it contains a higher amount of ash.

(vii) The slow stabilization is a limitation of the whole process especially for organosolv lignin, however, there are ways to accelerate it, e.g. by adding $H_3PO_4$ in the electrospinning solution, or with iodine treatment of the precursor fibers.

(viii) A very important feature of lignin-based CNFs is the interconnection among the fibers which comes as a result of controlled fusion. By adjusting this degree of interconnection, the electrical conductivity and the mechanical properties can be enhanced. However, excessive fusion compromises the surface area.

(ix) Lignin-based CNFs can be easily doped with metals, metal oxides, or nitrogen. Their surface chemistry can also be altered, e.g. through the anchoring of oxygen-containing functional groups. Doping generally improves their applicability in energy storage devices and in adsorption and catalysis.

(x) Limitations arise from the structural complexity of lignin, the presence of impurities, and its large polydispersity. Therefore, controlling its molecular structure, e.g. through fractionation, is desirable especially for improving the mechanical properties of CNFs.

(xi) Comparisons regarding the performance of CNFs in rechargeable batteries or supercapacitors based on values found in the literature are difficult since this depends on the choice of electrolytes and of the cathode materials. Nevertheless, lignin-based CNFs show a very promising potential for the manufacture of electrodes that can upgrade the current energy storage technology. First, they feature very high porosity which can be tailored during the manufacturing process. Micropores can accommodate a large number of ions and offer very high energy density and capacitance, while mesopores and interfiber voids facilitate the fast ion transport. Second, CNFs can be doped with metals in order to enhance their specific capacity/capacitance. Third, lignin-based CNFs can have a crucial role in the advancement of sodium-ion batteries. Fourth, lignin-based CNFs can be applied in flexible electronic devices. Finally, the most important is that the low cost and the large availability of lignin can reduce the cost of energy storage devices and contribute to the environmental protection.

Despite the limitations, lignin offers a very attractive option for the production of CNFs. The biggest advantage of lignin is



https://dx.doi.org/10.1021/acssuschemeng.0c03246
ACS Sustainable Chem. Eng. 2020, 8, 13868−13893

that it is a renewable, very abundant natural resource with relatively lower cost than PAN which is the most common CNF precursor. PAN, in contrast, is a petroleum-based polymer. In addition, lignin has a higher oxygen content which promotes the development of very high porosity. Compared to PAN, however, it presents lower yield during carbonization (<40 wt % compared to more than 50 wt % for PAN, depending on carbonization temperature), while its relatively low Mw translates into spinnability issues which require the presence of a binder polymer of higher Mw. The presence of impurities and ash in lignin raises the need of purification, while its irregular structure generally produces CNFs with more disordered structure and worse mechanical properties than PAN-based CNFs.

The future prospect of the widespread use of lignin-based CNFs, especially in energy-related applications, depends on the viability of their mass production. This is closely related to overcoming the limitations of the electrospinning technique. The versatility of this technique and the ease of producing nanosized fibers from a huge number of polymers has rendered it the most important nanofiber manufacturing technique. Nevertheless, its advantages are most often demonstrated at a laboratory scale with simple setups of a single needle. The low throughput of this setup (typically <1 g/h[114]) is unsuitable for the industrial scale-up and for the cost-effective mass production of nanofibers. In the recent years, intensive attempts to develop alternative setups or configurations that will offer high productivity have been proposed, and this prospect seems feasible. These setups include multineedle electrospinning, electroblowing, rotating spinnerets, and various configurations of free surface (needleless) electrospinning with stationary or moving spinnerets which can increase the productivity by 2 orders of magnitude.[113−116] Besides the increased productivity, advanced systems of quality control are also necessary for mass production.[115] Various companies are already working toward these directions, and they are commercializing their proprietary technologies.[115] Except for the productivity problem, the strategies of carbonization and activation are well-established and they have been used industrially for a long time now for commercial activated carbon. Hence, the continuous progress in the electrospinning technology offers well-grounded prospects for the industrial production of lignin-based CNFs.

Another trend that has emerged in the manufacture of nanofibers via electrospinning is the production of different hierarchical fibrous architectures. The vast majority of lignin-based CNFs summarized in this article use the classic 2D nonwoven electrospun mats which consist of tightly packed layers of randomly oriented nanofibers. However, recent variations of the technique allow the production of 3D scaffolds and aerogels and also woven fibers in aligned or crossed arrangements.[117,118] While the effect of the nanofibrous arrangement in the properties of CNFs is usually overlooked, certain examples from the articles summarized here prove that it can influence the electrical conductivity, the mechanical properties and the interfiber channels. Therefore, the increasing tendency of precise morphology control can open new possibilities for future applications of lignin-based CNFs.

While the vast majority of the body of research summarized here describes the application of lignin-based CNFs for energy storage, their performance in other fields would be interesting, as well. Other potential applications of lignin-based CNF are biomedical applications such as tissue engineering and controlled drug delivery, environmental applications such as wastewater treatment and air purification, electromagnetic interference shielding, and shape memory materials.[119] In addition, the wider use of these materials in catalysis is suggested. With regards to energy storage, these materials are attractive not only for LIBs, SIBs, and supercapacitors but also for the manufacture of electrodes for other devices such as Li−S batteries, K-ion batteries, metal−air batteries, and fuel cells. CNFs produced from other precursors, mainly PAN, have already appeared in these devices.[119,120] Lignin, however, can offer high-performance CNFs at lower cost. Depending on industrially scalable electrospinning setups, lignin-based CNFs can, therefore, advance the existing energy storage technology, promote the use of electric vehicles, and contribute to environmental protection.

Replacing benchmark materials or long-standing processes is a difficult task that requires the consideration of the cost arising from the disruption of established industrial practice. Nevertheless, the flexibility arising from using lignin as a precursor allows the design of "bespoke" CNFs instead of relying to "off-the-shelf" solutions. Furthermore, the long-term benefits of promoting a sustainable, circular economy should be decisive factors in the upgrade of existing technology.

## AUTHOR INFORMATION


### Corresponding Author

**Ioannis Zuburtikudis** − *Department of Chemical Engineering, Abu Dhabi University, Abu Dhabi 59911, U.A.E.*; Email: ioannis.zuburtikudis@adu.ac.ae

### Authors

**Efstratios Svinterikos** − *Department of Chemical and Petroleum Engineering, United Arab Emirates University (U.A.E.U.), Al Ain 15551, U.A.E.*; orcid.org/0000-0001-6303-8944

**Mohamed Al-Marzouqi** − *Department of Chemical and Petroleum Engineering, United Arab Emirates University (U.A.E.U.), Al Ain 15551, U.A.E.*

Complete contact information is available at: https://pubs.acs.org/10.1021/acssuschemeng.0c03246


### Notes

The authors declare no competing financial interest.

### Biographies

Dr. Efstratios Svinterikos had just completed his Ph.D. in Chemical Engineering at the United Arab Emirates University. In his Ph.D.



https://dx.doi.org/10.1021/acssuschemeng.0c03246
ACS Sustainable Chem. Eng. 2020, 8, 13868−13893

research, he proposed a new route for the manufacture of high added-value products from renewable and waste resources, by combining lignin with recycled-PET for the production of electrospun-based activated carbon nanofibers (ACNFs). He used these ACNFs successfully for the adsorptive desulfurization of fossil fuels. Efstratios holds a B.Sc. in Chemical Engineering from the National Technical University of Athens, Greece, and a M.Sc. in Materials Science and Technology from the Aristotle University of Thessaloniki, Greece.

Prof. Ioannis Zuburtikudis is currently with the Chemical Engineering Department of Abu Dhabi University and acts as its Chair. He studied Chemical Engineering in Greece and in the USA, where he worked as a Research Scientist before joining the Greek Academia and establishing the NanoMaterials & Manufacturing Processes Laboratory (www.nanohybrid.eu). His research lies in the nexus of nanotechnology, catalytic chemical reaction engineering, soft-matter, and sustainability. He has been granted various research grants by Greek, EU, and UAE agencies. He has authored over two hundred articles in refereed journals and conference proceedings and has co-organized International, European, and Greek conferences, while he has supervised many undergraduate and graduate students.

Prof. Mohamed Al-Marzouqi obtained his B.Sc. and M.Sc. from Washington State University and Ph.D. from Oregon State University, all in chemical engineering. His specialization is in the areas of membrane gas separation, sustainability, and environmental engineering. Prof. Al-Marzouqi joined Chemical & Petroleum Engineering Department at the United Arab Emirates University in 1996. Prof. Al-Marzouqi has 3 patents, over 70 journal publications, 2 book chapters, and more than 75 local and international conference presentations.

## ■ ACKNOWLEDGMENTS

The authors would like to acknowledge the financial support provided by the Emirates Center for Energy and Environment Research (grant number 31R147).

## ■ REFERENCES

(1) Laurichesse, S.; Avérous, L. Chemical Modification of Lignins: Towards Biobased Polymers. *Prog. Polym. Sci.* **2014**, *39* (7), 1266−1290.
(2) Figueiredo, P.; Lintinen, K.; Hirvonen, J. T.; Kostiainen, M. A.; Santos, H. A. Properties and Chemical Modifications of Lignin: Towards Lignin-Based Nanomaterials for Biomedical Applications. *Prog. Mater. Sci.* **2018**, *93*, 233−269.
(3) Duval, A.; Lawoko, M. A Review on Lignin-Based Polymeric, Micro- and Nano-Structured Materials. *React. Funct. Polym.* **2014**, *85*, 78−96.
(4) Feofilova, E. P.; Mysyakina, I. S. Lignin: Chemical Structure, Biodegradation, and Practical Application (a Review). *Appl. Biochem. Microbiol.* **2016**, *52* (6), 573−581.
(5) Hu, S.; Hsieh, Y.-L. Ultrafine Microporous and Mesoporous Activated Carbon Fibers from Alkali Lignin. *J. Mater. Chem. A* **2013**, *1*, 11279.
(6) Baker, D. A.; Rials, T. G. Recent Advances in Low-Cost Carbon Fiber Manufacture from Lignin. *J. Appl. Polym. Sci.* **2013**, *130* (2), 713−728.
(7) Wang, X.; Zhang, W.; Chen, M.; Zhou, X. Electrospun Enzymatic Hydrolysis Lignin-Based Carbon Nanofibers as Binder-Free Supercapacitor Electrodes with High Performance. *Polymers* **2018**, *10*, 1306.
(8) Wang, X.; Xu, Q.; Cheng, J.; Hu, G.; Xie, X.; Peng, C.; Yu, X.; Shen, H.; Zhao, Z. K.; Xie, H. Bio-Refining Corn Stover into Microbial Lipid and Advanced Energy Material Using Ionic Liquid-Based Organic Electrolyte. *Ind. Crops Prod.* **2020**, *145*, 112137.
(9) Kai, D.; Tan, M. J.; Chee, P. L.; Chua, Y. K.; Yap, Y. L.; Loh, X. J. Towards Lignin-Based Functional Materials in a Sustainable World. *Green Chem.* **2016**, *18* (5), 1175−1200.
(10) Ghosh, T.; Chen, J.; Kumar, A.; Tang, T.; Ayranci, C. Bio-Cleaning Improves the Mechanical Properties of Lignin-Based Carbon Fibers. *RSC Adv.* **2020**, *10* (39), 22983−22995.
(11) Frank, E.; Steudle, L. M.; Ingildeev, D.; Spörl, J. M.; Buchmeiser, M. R. Carbon Fibers: Precursor Systems, Processing, Structure, and Properties. *Angew. Chem., Int. Ed.* **2014**, *53* (21), 5262−5298.
(12) Svinterikos, E.; Zuburtikudis, I.; Al-Marzouqi, M. The Nanoscale Dimension Determines the Carbonization Outcome of Electrospun Lignin/Recycled-PET Fibers. *Chem. Eng. Sci.* **2019**, *202*, 26−35.
(13) Zhang, B.; Kang, F.; Tarascon, J. M.; Kim, J. K. Recent Advances in Electrospun Carbon Nanofibers and Their Application in Electrochemical Energy Storage. *Prog. Mater. Sci.* **2016**, *76*, 319−380.
(14) Ogale, A. A.; Zhang, M.; Jin, J. Recent Advances in Carbon Fibers Derived from Biobased Precursors. *J. Appl. Polym. Sci.* **2016**, *133* (45), 43794.
(15) Li, W.; Li, M.; Adair, K. R.; Sun, X.; Yu, Y. Carbon Nanofiber-Based Nanostructures for Lithium-Ion and Sodium-Ion Batteries. *J. Mater. Chem. A* **2017**, *5* (27), 13882−13906.
(16) Marsh, H.; Rodríguez-Reinoso, F. *Activated Carbon* **2006**, 13.
(17) Marsh, H.; Rodríguez-Reinoso, F. Porosity in Carbons: Modeling. *Activated Carbon* **2006**, 87.
(18) Ko, F.; Wan, Y. *Introduction to Nanofiber Materials*; Cambridge University Press, 2014; Chapter 3.
(19) Zhang, L.; Aboagye, A.; Kelkar, A.; Lai, C.; Fong, H. A Review: Carbon Nanofibers from Electrospun Polyacrylonitrile and Their Applications. *J. Mater. Sci.* **2014**, *49*, 463−480.
(20) Svinterikos, E.; Zuburtikudis, I.; Al-Marzouqi, M. Carbon Nanomaterials for the Adsorptive Desulfurization of Fuels. *J. Nanotechnol.* **2019**, *2019*, 2809867.


https://dx.doi.org/10.1021/acssuschemeng.0c03246
*ACS Sustainable Chem. Eng.* 2020, 8, 13868−13893

(21) Scrosati, B.; Hassoun, J.; Sun, Y. K. Lithium-Ion Batteries. A Look into the Future. *Energy Environ. Sci.* **2011**, *4* (9), 3287−3295.
(22) Goodenough, J. B.; Park, K. S. The Li-Ion Rechargeable Battery: A Perspective. *J. Am. Chem. Soc.* **2013**, *135* (4), 1167−1176.
(23) Sharma, S.; Panwar, A. K.; Tripathi, M. M. Storage Technologies for Electric Vehicles. *J. Traffic Transp. Eng. (English ed.)* **2020**, *7* (3), 340−361.
(24) https://www.fueleconomy.gov/ (accessed 20th July 2020).
(25) https://www.forbes.com/sites/greatspeculations/2020/01/13/how-battery-costs-impact-teslas-margins-an-interactive-analysis/#1226fa115036 (accessed on 20th July 2020).
(26) https://about.bnef.com/blog/behind-scenes-take-lithium-ion-battery-prices/ (accessed on 20th July 2020).
(27) Manthiram, A. A Reflection on Lithium-Ion Battery Cathode Chemistry. *Nat. Commun.* **2020**, *11* (1), 1−9.
(28) Liu, L.; Niu, Z.; Chen, J. Unconventional Supercapacitors from Nanocarbon-Based Electrode Materials to Device Configurations. *Chem. Soc. Rev.* **2016**, *45* (15), 4340−4363.
(29) Slater, M. D.; Kim, D.; Lee, E.; Johnson, C. S. Sodium-Ion Batteries. *Adv. Funct. Mater.* **2013**, *23* (8), 947−958.
(30) https://tradingeconomics.com/commodity/soda-ash (accessed on 20th March 2020).
(31) https://www.fastmarkets.com/commodities/industrial-minerals/lithium-price-spotlight (accessed on 20th March 2020).
(32) Beda, A.; Taberna, P. L.; Simon, P.; Matei Ghimbeu, C. Hard Carbons Derived from Green Phenolic Resins for Na-Ion Batteries. *Carbon* **2018**, *139*, 248−257.
(33) Borchardt, L.; Oschatz, M.; Kaskel, S. Tailoring Porosity in Carbon Materials for Supercapacitor Applications. *Mater. Horiz.* **2014**, *1* (2), 157−168.
(34) Frackowiak, E.; Béguin, F. Carbon Materials for the Electrochemical Storage of Energy in Capacitors. *Carbon* **2001**, *39* (6), 937−950.
(35) Herou, S.; Schlee, P.; Jorge, A. B.; Titirici, M. Biomass-Derived Electrodes for Flexible Supercapacitors. *Curr. Opin. Green Sustain. Chem.* **2018**, *9*, 18−24.
(36) Jeong, J. H.; Lee, Y. H.; Kim, B. H. Relationship between Microstructure and Electrochemical Properties of 2lignin-Derived Carbon Nanofibers Prepared by Thermal Treatment. *Synth. Met.* **2020**, *260*, 116287.
(37) Lai, C.; Zhou, Z.; Zhang, L.; Wang, X.; Zhou, Q.; Zhao, Y.; Wang, Y.; Wu, X. F.; Zhu, Z.; Fong, H. Free-Standing and Mechanically Flexible Mats Consisting of Electrospun Carbon Nanofibers Made from a Natural Product of Alkali Lignin as Binder-Free Electrodes for High-Performance Supercapacitors. *J. Power Sources* **2014**, *247*, 134−141.
(38) Ma, X.; Smirnova, A. L.; Fong, H. Flexible Lignin-Derived Carbon Nanofiber Substrates Functionalized with Iron (III) Oxide Nanoparticles as Lithium-Ion Battery Anodes. *Mater. Sci. Eng., B* **2019**, *241*, 100−104.
(39) Zhao, Y.; Liu, Y.; Tong, C.; Ru, J.; Geng, B.; Ma, Z.; Liu, H.; Wang, L. Flexible Lignin-Derived Electrospun Carbon Nanofiber Mats as a Highly Efficient and Binder-Free Counter Electrode for Dye-Sensitized Solar Cells. *J. Mater. Sci.* **2018**, *53* (10), 7637−7647.
(40) Wei, J.; Geng, S.; Pitkänen, O.; Järvinen, T.; Kordas, K.; Oksman, K. Green Carbon Nanofiber Networks for Advanced Energy Storage. *ACS Appl. Energy Mater.* **2020**, *3* (4), 3530−3540.
(41) Ko, F.; Wan, Y. *Introduction to Nanofiber Materials*; Cambridge University Press, 2014; Chapter 9.
(42) Inagaki, M.; Yang, Y.; Kang, F. Carbon Nanofibers Prepared via Electrospinning. *Adv. Mater.* **2012**, *24* (19), 2547−2566.
(43) Svinterikos, E.; Zuburtikudis, I. Carbon Nanofibers from Renewable Bioresources (Lignin) and a Recycled Commodity Polymer [Poly(Ethylene Terephthalate)]. *J. Appl. Polym. Sci.* **2016**, *133*, 43936.
(44) Wang, H. G.; Yuan, S.; Ma, D. L.; Zhang, X. B.; Yan, J. M. Electrospun Materials for Lithium and Sodium Rechargeable Batteries: From Structure Evolution to Electrochemical Performance. *Energy Environ. Sci.* **2015**, *8* (6), 1660−1681.
(45) Zhang, C. L.; Yu, S. H. Nanoparticles Meet Electrospinning: Recent Advances and Future Prospects. *Chem. Soc. Rev.* **2014**, *43* (13), 4423−4448.
(46) Fan, Q.; Ma, C.; Wu, L.; Wei, C.; Wang, H.; Song, Y.; Shi, J. Preparation of Cellulose Acetate Derived Carbon Nanofibers by $ZnCl_2$ Activation as a Supercapacitor Electrode. *RSC Adv.* **2019**, *9* (12), 6419−6428.
(47) Cai, J.; Niu, H.; Wang, H.; Shao, H.; Fang, J.; He, J.; Xiong, H.; Ma, C.; Lin, T. High-Performance Supercapacitor Electrode from Cellulose-Derived, Inter-Bonded Carbon Nanofibers. *J. Power Sources* **2016**, *324*, 302−308.
(48) Lallave, M.; Bedia, J.; Ruiz-Rosas, R.; Rodríguez-Mirasol, J.; Cordero, T.; Otero, J. C.; Marquez, M.; Barrero, A.; Loscertales, I. G. Filled and Hollow Carbon Nanofibers by Coaxial Electrospinning of Alcell Lignin without Binder Polymers. *Adv. Mater.* **2007**, *19* (23), 4292−4296.
(49) Schlee, P.; Hosseinaei, O.; Baker, D.; Landmer, A.; Tomani, P.; Mostazo-Lopez, M.; Cazorla-Amoros, D.; Herou, S.; Titirici, M.-M. From Waste to Wealth: From Kraft Lignin to Free-Standing Supercapacitors. *Carbon* **2019**, *145*, 470−480.
(50) García-Mateos, F. J.; Cordero-Lanzac, T.; Berenguer, R.; Morallón, E.; Cazorla-Amorós, D.; Rodríguez-Mirasol, J.; Cordero, T. Lignin-Derived Pt Supported Carbon (Submicron)Fiber Electrocatalysts for Alcohol Electro-Oxidation. *Appl. Catal., B* **2017**, *211*, 18−30.
(51) García-Mateos, F. J.; Berenguer, R.; Valero-Romero, M. J.; Rodríguez-Mirasol, J.; Cordero, T. Phosphorus Functionalization for the Rapid Preparation of Highly Nanoporous Submicron-Diameter Carbon Fibers by Electrospinning of Lignin Solutions. *J. Mater. Chem. A* **2018**, *6* (3), 1219−1233.
(52) You, X.; Koda, K.; Yamada, T.; Uraki, Y. Preparation of Electrode for Electric Double Layer Capacitor from Electrospun Lignin Fibers. *Holzforschung* **2015**, *69* (9), 1097−1106.
(53) Ruiz-Rosas, R.; Bedia, J.; Lallave, M.; Loscertales, I. G.; Barrero, A.; Rodriguez-Mirasol, J.; Cordero, T.; Rodríguez-Mirasol, J.; Cordero, T. The Production of Submicron Diameter Carbon Fibers by the Electrospinning of Lignin. *Carbon* **2010**, *48* (3), 696−705.
(54) Dalton, N.; Lynch, R. P.; Collins, M. N.; Culebras, M. Thermoelectric Properties of Electrospun Carbon Nanofibres Derived from Lignin. *Int. J. Biol. Macromol.* **2019**, *121*, 472−479.
(55) Cho, M.; Karaaslan, M.; Wang, H.; Renneckar, S. Greener Transformation of Lignin into Ultralight Multifunctional Materials. *J. Mater. Chem. A* **2018**, *6* (42), 20973−20981.
(56) García-Mateos, F. J.; Ruiz-Rosas, R.; María Rosas, J.; Morallón, E.; Cazorla-Amorós, D.; Rodríguez-Mirasol, J.; Cordero, T. Activation of Electrospun Lignin-Based Carbon Fibers and Their Performance as Self-Standing Supercapacitor Electrodes. *Sep. Purif. Technol.* **2020**, *241*, 116724.
(57) Jin, J.; Yu, B. J.; Shi, Z. Q.; Wang, C. Y.; Chong, C. B. Lignin-Based Electrospun Carbon Nanofibrous Webs as Free-Standing and Binder-Free Electrodes for Sodium Ion Batteries. *J. Power Sources* **2014**, *272*, 800−807.
(58) Shi, Z.; Jin, G.; Wang, J.; Zhang, J. Free-Standing, Welded Mesoporous Carbon Nanofibers as Anode for High-Rate Performance Li-Ion Batteries. *J. Electroanal. Chem.* **2017**, *795*, 26−31.
(59) Perera Jayawickramage, R. A.; Balkus, K. J.; Ferraris, J. P. Binder Free Carbon Nanofiber Electrodes Derived from Polyacrylonitrile-Lignin Blends for High Performance Supercapacitors. *Nanotechnology* **2019**, *30* (35), 355402.
(60) Yun, S. I.; Kim, S. H.; Kim, D. W.; Kim, Y. A.; Kim, B. H. Facile Preparation and Capacitive Properties of Low-Cost Carbon Nanofibers with ZnO Derived from Lignin and Pitch as Supercapacitor Electrodes. *Carbon* **2019**, *149*, 637−645.
(61) Lei, D.; Li, X. D.; Seo, M. K.; Khil, M. S.; Kim, H. Y.; Kim, B. S. $NiCo_2O_4$ Nanostructure-Decorated PAN/Lignin Based Carbon Nanofiber Electrodes with Excellent Cyclability for Flexible Hybrid Supercapacitors. *Polymer* **2017**, *132*, 31−40.


https://dx.doi.org/10.1021/acssuschemeng.0c03246
*ACS Sustainable Chem. Eng.* 2020, 8, 13868−13893

(62) Dai, Z.; Ren, P. G.; Jin, Y. L.; Zhang, H.; Ren, F.; Zhang, Q. Nitrogen-Sulphur Co-Doped Graphenes Modified Electrospun Lignin/Polyacrylonitrile-Based Carbon Nanofiber as High Performance Supercapacitor. *J. Power Sources* **2019**, *437*, 226937.
(63) Demiroğlu Mustafov, S.; Mohanty, A. K.; Misra, M.; Seydibeyoğlu, M. Ö. Fabrication of Conductive Lignin/PAN Carbon Nanofiber with Enhanced Graphene for the Modified Electrode. *Carbon* **2019**, *147*, 262−275.
(64) Park, C. W.; Youe, W. J.; Han, S. Y.; Kim, Y. S.; Lee, S. H. Characteristics of Carbon Nanofibers Produced from Lignin/Polyacrylonitrile (PAN)/Kraft Lignin-g-PAN Copolymer Blends Electrospun Nanofibers. *Holzforschung* **2017**, *71* (9), 743−750.
(65) Ma, A.; Zhou, L.; Chang, J. Conversion of Lignin-Nanofibers to CNFs. *Nano* **2015**, *10* (6), 1−9.
(66) Xu, X.; Zhou, J.; Jiang, L.; Lubineau, G.; Chen, Y.; Wu, X. F.; Piere, R. Porous Core-Shell Carbon Fibers Derived from Lignin and Cellulose Nanofibrils. *Mater. Lett.* **2013**, *109*, 175−178.
(67) Xu, X.; Zhou, J.; Jiang, L.; Lubineau, G.; Payne, S. A.; Gutschmidt, D. Lignin-Based Carbon Fibers: Carbon Nanotube Decoration and Superior Thermal Stability. *Carbon* **2014**, *80*, 91−102.
(68) Youe, W. J.; Lee, S. M.; Lee, S. S.; Lee, S. H.; Kim, Y. S. Characterization of Carbon Nanofiber Mats Produced from Electrospun Lignin-g-Polyacrylonitrile Copolymer. *Int. J. Biol. Macromol.* **2016**, *82*, 497−504.
(69) Nordin, N. A.; Abdul Rahman, N.; Abdullah, A. H. Effective Removal of Pb(II) Ions by Electrospun PAN/Sago Lignin-Based Activated Carbon Nanofibers. *Molecules* **2020**, *25*, 3081.
(70) Zhang, W.; Yang, P.; Luo, M.; Wang, X.; Zhang, T.; Chen, W.; Zhou, X. Fast Oxygen, Nitrogen Co-Functionalization on Electrospun Lignin-Based Carbon Nanofibers Membrane via Air Plasma for Energy Storage Application. *Int. J. Biol. Macromol.* **2020**, *143*, 434−442.
(71) Zhang, X.; Dong, S.; Wu, W.; Yang, J.; Li, J.; Shi, K.; Liu, H. Influence of Lignin Units on the Properties of Lignin/PAN-Derived Carbon Fibers. *J. Appl. Polym. Sci.* **2020**, *137*, 49274.
(72) Du, B.; Chen, C.; Sun, Y.; Yu, M.; Liu, B.; Wang, X.; Zhou, J. Lignin Bio-Oil-Based Electrospun Nanofibers with High Substitution Ratio Property for Potential Carbon Nanofibers Applications. *Polym. Test.* **2020**, *89*, 106591.
(73) Choi, D. I.; Lee, J.-N.; Song, J.; Kang, P.-H.; Park, J.-K.; Lee, Y. M. Fabrication of Polyacrylonitrile/Lignin-Based Carbon Nanofibers for High-Power Lithium Ion Battery Anodes. *J. Solid State Electrochem.* **2013**, *17* (9), 2471−2475.
(74) Dai, Z.; Shi, X.; Liu, H.; Li, H.; Han, Y.; Zhou, J. High-Strength Lignin-Based Carbon Fibers via a Low-Energy Method. *RSC Adv.* **2018**, *8* (3), 1218−1224.
(75) Ding, R.; Wu, H.; Thunga, M.; Bowler, N.; Kessler, M. R. Processing and Characterization of Low-Cost Electrospun Carbon Fibers from Organosolv Lignin/Polyacrylonitrile Blends. *Carbon* **2016**, *100*, 126−136.
(76) Zhang, R.; Du, Q.; Wang, L.; Zheng, Z.; Guo, L.; Zhang, X.; Yang, X.; Yu, H. Unlocking the Response of Lignin Structure for Improved Carbon Fiber Production and Mechanical Strength. *Green Chem.* **2019**, *21* (18), 4981−4987.
(77) Beck, R. J.; Zhao, Y.; Fong, H.; Menkhaus, T. J. Electrospun Lignin Carbon Nanofiber Membranes with Large Pores for Highly Efficient Adsorptive Water Treatment Applications. *J. Water Process Eng.* **2017**, *16*, 240−248.
(78) Ma, X.; Kolla, P.; Zhao, Y.; Smirnova, A. L.; Fong, H. Electrospun Lignin-Derived Carbon Nanofiber Mats Surface-Decorated with $MnO_2$ Nanowhiskers as Binder-Free Supercapacitor Electrodes with High Performance. *J. Power Sources* **2016**, *325*, 541−548.
(79) Lai, C.; Kolla, P.; Zhao, Y.; Fong, H.; Smirnova, A. L. Lignin-Derived Electrospun Carbon Nanofiber Mats with Supercritically Deposited Ag Nanoparticles for Oxygen Reduction Reaction in Alkaline Fuel Cells. *Electrochim. Acta* **2014**, *130*, 431−438.
(80) Stojanovska, E.; Pampal, E. S.; Kilic, A.; Quddus, M.; Candan, Z. Developing and Characterization of Lignin-Based Fibrous Nanocarbon Electrodes for Energy Storage Devices. *Composites, Part B* **2019**, *158*, 239−248.
(81) Perera Jayawickramage, R. A.; Ferraris, J. P. High Performance Supercapacitors Using Lignin Based Electrospun Carbon Nanofiber Electrodes in Ionic Liquid Electrolytes. *Nanotechnology* **2019**, *30* (15), 155402.
(82) Ago, M.; Borghei, M.; Haataja, J. S.; Rojas, O. J. Mesoporous Carbon Soft-Templated from Lignin Nanofiber Networks: Microphase Separation Boosts Supercapacitance in Conductive Electrodes. *RSC Adv.* **2016**, *6* (89), 85802−85810.
(83) Roman, J.; Neri, W.; Derré, A.; Poulin, P. Electrospun Lignin-Based Twisted Carbon Nanofibers for Potential Microelectrodes Applications. *Carbon* **2019**, *145*, 556−564.
(84) Song, M.; Yu, L.; Song, B.; Meng, F.; Tang, X. Alkali Promoted the Adsorption of Toluene by Adjusting the Surface Properties of Lignin-Derived Carbon Fibers. *Environ. Sci. Pollut. Res.* **2019**, *26* (22), 22284−22294.
(85) Meng, F.; Song, M.; Wei, Y.; Wang, Y. The Contribution of Oxygen-Containing Functional Groups to the Gas-phase Adsorption of Volatile Organic Compounds with Different Polarities onto Lignin-derived Activated Carbon Fibers. *Environ. Sci. Pollut. Res.* **2019**, *26* (7), 7195−7204.
(86) Song, M.; Zhang, W.; Chen, Y.; Luo, J.; Crittenden, J. The Preparation and Performance of Lignin-Based Activated Carbon Fiber Adsorbents for Treating Gaseous Streams. *Front. Chem. Sci. Eng.* **2017**, *11* (3), 328−337.
(87) Guo, C.; Ma, H.; Zhang, Q.; Li, M.; Jiang, H.; Chen, C.; Wang, S.; Min, D. Nano $MnO_2$ Radially Grown on Lignin-Based Carbon Fiber by One-Step Solution Reaction for Supercapacitors with High Performance. *Nanomaterials* **2020**, *10* (3), 594.
(88) Wei, Y.; Song, M.; Yu, L.; Tang, X. Preparation of ZnO-Loaded Lignin-Based Carbon Fiber for the Electrocatalytic Oxidation of Hydroquinone. *Catalysts* **2017**, *7* (6), 180.
(89) Yu, B.; Gele, A.; Wang, L. Iron Oxide/Lignin-Based Hollow Carbon Nanofibers Nanocomposite as an Application Electrode Materials for Supercapacitors. *Int. J. Biol. Macromol.* **2018**, *118*, 478−484.
(90) Dallmeyer, I.; Lin, L. T.; Li, Y.; Ko, F.; Kadla, J. F. Preparation and Characterization of Interconnected, Kraft Lignin-Based Carbon Fibrous Materials by Electrospinning. *Macromol. Mater. Eng.* **2014**, *299*, 540−551.
(91) Schlee, P.; Herou, S.; Jervis, R.; Shearing, P. R.; Brett, D. J. L.; Baker, D.; Hosseinaei, O.; Tomani, P.; Murshed, M. M.; Li, Y.; et al. Free-Standing Supercapacitors from Kraft Lignin Nanofibers with Remarkable Volumetric Energy Density. *Chem. Sci.* **2019**, *10* (10), 2980−2988.
(92) Shi, X.; Wang, X.; Tang, B.; Dai, Z.; Chen, K.; Zhou, J. Impact of Lignin Extraction Methods on Microstructure and Mechanical Properties of Lignin-Based Carbon Fibers. *J. Appl. Polym. Sci.* **2018**, *135* (10), 1−7.
(93) Hu, S.; Jiang, F.; Hsieh, Y.-L. 1D Lignin-Based Solid Acid Catalysts for Cellulose Hydrolysis to Glucose and Nanocellulose. *ACS Sustainable Chem. Eng.* **2015**, *3*, 2566−2574.
(94) Aslanzadeh, S.; Ahvazi, B.; Boluk, Y.; Ayranci, C. Carbon Fiber Production from Electrospun Sulfur Free Softwood Lignin Precursors. *J. Eng. Fibers Fabr.* **2017**, *12* (4), 33−43.
(95) Choi, J.; Yang, H.; Ko, F.; Chan, S.; Chung, W.; Kim, S. S. Fabrication and Characterization of Palladium Nanoparticle Reinforced Multifunctional Lignin Nanofiber Mat. *J. Nanosci. Nanotechnol.* **2016**, *16* (10), 11046−11051.
(96) Hu, S.; Zhang, S.; Pan, N.; Hsieh, Y. Lo. High Energy Density Supercapacitors from Lignin Derived Submicron Activated Carbon Fibers in Aqueous Electrolytes. *J. Power Sources* **2014**, *270*, 106−112.
(97) Liu, S.; Cheng, X.; He, Z.; Liu, J.; Zhang, X.; Xu, J.; Lei, C. Amine-Terminated Highly Cross-Linked Polyphosphazene-Functionalized Carbon Nanotube-Reinforced Lignin-Based Electrospun


https://dx.doi.org/10.1021/acssuschemeng.0c03246
ACS Sustainable Chem. Eng. 2020, 8, 13868−13893

Carbon Nanofibers. *ACS Sustainable Chem. Eng.* **2020**, *8* (4), 1840−1849.
(98) Dai, Z.; Ren, P.; Cao, Q.; Gao, X.; He, W.; Xiao, Y.; Jin, Y.; Ren, F. Synthesis of TiO2@lignin Based Carbon Nanofibers Composite Materials with Highly Efficient Photocatalytic to Methylene Blue Dye. *J. Polym. Res.* **2020**, DOI: 10.1007/s10965-020-02068-7.
(99) Vivo-Vilches, J. F.; Celzard, A.; Fierro, V.; Devin-Ziegler, I.; Brosse, N.; Dufour, A.; Etienne, M. Lignin-Based Carbon Nanofibers as Electrodes for Vanadium Redox Couple Electrochemistry. *Nanomaterials* **2019**, *9* (1), 1−13.
(100) Wang, S. X.; Yang, L.; Stubbs, L. P.; Li, X.; He, C. Lignin-Derived Fused Electrospun Carbon Fibrous Mats as High Performance Anode Materials for Lithium Ion Batteries. *ACS Appl. Mater. Interfaces* **2013**, *5* (23), 12275−12282.
(101) Wang, L.; Aorigele; Sun, Y. Preparation of Iron Oxide Particle-Decorated Lignin-Based Carbon Nanofibers as Electrode Material for Pseudocapacitor. *J. Wood Chem. Technol.* **2017**, *37* (6), 423−432.
(102) Cho, M.; Karaaslan, M.; Chowdhury, S.; Ko, F.; Renneckar, S. Skipping Oxidative Thermal Stabilization for Lignin-Based Carbon Nanofibers. *ACS Sustainable Chem. Eng.* **2018**, *6* (5), 6434−6444.
(103) Wang, S.; Innocent, M. T.; Wang, Q.; Xiang, H.; Tang, J.; Zhu, M. Kraft Lignin-Based Piezoresistive Sensors: Effect of Chemical Structure on the Microstructure of Ultrathin Carbon Fibers. *Int. J. Biol. Macromol.* **2020**, *151*, 730−739.
(104) Hérou, S.; Crespo, M.; Titirici, M. Investigating the Effects of Activating Agent Morphology on the Porosity and Related Capacitance of Nanoporous Carbons. *CrystEngComm* **2020**, *22* (9), 1560−1567.
(105) Guo, Z.; Liu, Z.; Ye, L.; Ge, K.; Zhao, T. The Production of Lignin-Phenol-Formaldehyde Resin Derived Carbon Fibers Stabilized by BN Preceramic Polymer. *Mater. Lett.* **2015**, *142*, 49−51.
(106) Ma, C.; Li, Z.; Li, J.; Fan, Q.; Wu, L.; Shi, J.; Song, Y. Lignin-Based Hierarchical Porous Carbon Nanofiber Films with Superior Performance in Supercapacitors. *Appl. Surf. Sci.* **2018**, *456*, 568−576.
(107) Cao, M.; Cheng, W.; Ni, X.; Hu, Y.; Han, G. Lignin-Based Multi-Channels Carbon Nanofibers @ $SnO_2$ Nanocomposites for High-Performance Supercapacitors. *Electrochim. Acta* **2020**, *345*, 136172.
(108) Schreiber, M.; Vivekanandhan, S.; Mohanty, A. K.; Misra, M. Iodine Treatment of Lignin−Cellulose Acetate Electrospun Fibers: Enhancement of Green Fiber Carbonization. *ACS Sustainable Chem. Eng.* **2015**, *3* (1), 33.
(109) Cao, Q.; Zhang, Y.; Chen, J.; Zhu, M.; Yang, C.; Guo, H.; Song, Y.; Li, Y.; Zhou, J. Electrospun Biomass Based Carbon Nanofibers as High-Performance Supercapacitors. *Ind. Crops Prod.* **2020**, *148*, 112181.
(110) Jia, H.; Sun, N.; Dirican, M.; Li, Y.; Chen, C.; Zhu, P.; Yan, C.; Zang, J.; et al. Electrospun Kraft Lignin-Cellulose Acetate Derived a Nano Carbon Network as an Anode for High-Performance Sodium-Ion Batteries. *ACS Appl. Mater. Interfaces* **2018**, *10* (51), 44368−44375.
(111) Svinterikos, E.; Zuburtikudis, I.; Al-Marzouqi, M. Fabricating Carbon Nanofibers from a Lignin/r-PET Blend: The Synergy of Mass Ratio with the Average Fiber Diameter. *Appl. Nanosci.* **2020**, *10*, 1331−1343.
(112) Kubo, S.; Kadla, J. F. Kraft Lignin/Poly(Ethylene Oxide) Blends: Effect of Lignin Structure on Miscibility and Hydrogen Bonding. *J. Appl. Polym. Sci.* **2005**, *98* (3), 1437−1444.
(113) Deng, L.; Young, R. J.; Kinloch, I. A.; Zhu, Y.; Eichhorn, S. J. Carbon Nanofibres Produced from Electrospun Cellulose Nanofibres. *Carbon* **2013**, *58* (0), 66−75.
(114) Vass, P.; Szabó, E.; Domokos, A.; Hirsch, E.; Galata, D.; Farkas, B.; Démuth, B.; Andersen, S. K.; Vigh, T.; Verreck, G.; et al. Scale-up of Electrospinning Technology: Applications in the Pharmaceutical Industry. *Wiley Interdiscip. Rev.: Nanomed. Nanobiotechnol.* **2020**, *12* (4), 1−24.
(115) Persano, L.; Camposeo, A.; Tekmen, C.; Pisignano, D. Industrial Upscaling of Electrospinning and Applications of Polymer Nanofibers: A Review. *Macromol. Mater. Eng.* **2013**, *298*, 504−520.
(116) Song, J.; Kim, M.; Lee, H. Recent Advances on Nanofiber Fabrications: Unconventional State-of-the-Art Spinning Techniques. *Polymers* **2020**, *12* (6), 1386.
(117) Chen, Y.; Shafiq, M.; Liu, M.; Morsi, Y.; Mo, X. Advanced Fabrication for Electrospun Three-Dimensional Nanofiber Aerogels and Scaffolds. *Bioactive Materials* **2020**, *5*, 963−979.
(118) Keirouz, A.; Chung, M.; Kwon, J.; Fortunato, G.; Radacsi, N. 2D and 3D Electrospinning Technologies for the Fabrication of Nanofibrous Scaffolds for Skin Tissue Engineering: A Review. *Wiley Interdiscip. Rev. Nanomedicine Nanobiotechnology* **2020**, *12* (4), 1−32.
(119) Zhou, X.; Wang, Y.; Gong, C.; Liu, B.; Wei, G. Production, Structural Design, Functional Control, and Broad Applications of Carbon Nanofiber-Based Nanomaterials: A Comprehensive Review. *Chem. Eng. J.* **2020**, *402*, 126189.
(120) Tong, Z.; Huang, L.; Lei, W.; Zhang, H.; Zhang, S. Carbon-Containing Electrospun Nanofibers for Lithium−Sulfur Battery: Current Status and Future Directions. *J. Energy Chem.* **2021**, *54*, 254−273.


https://dx.doi.org/10.1021/acssuschemeng.0c03246
*ACS Sustainable Chem. Eng.* 2020, 8, 13868−13893